Design and Control of a Voice Coil Actuated Robot Arm for Human-Robot Interaction

by

John M. McBean

B.S. Mechanical Engineering
Massachusetts Institute of Technology, 2001

SUBMITTED TO THE DEPARTMENT OF MECHANICAL ENGINEERING IN PARTIAL FULFILLMENT OF THE REQUIREMENTS FOR THE DEGREE OF

MASTER OF SCIENCE IN MECHANICAL ENGINEERING
AT THE
MASSACHUSETTS INSTITUTE OF TECHNOLOGY

JUNE 2004

Signature of Author.....
Department of Mechanical Engineering
May 7, 2004

Certified by.....
Cynthia Breazeal
Assistant Professor of Media Arts and Sciences
Thesis Supervisor

Approved by.....
Woodie Flowers
Pappalardo Professor of Mechanical Engineering
Mechanical Engineering Faculty Reader

Accepted by.....
Ain Sonin
Chairman, Department Committee on Graduate Students

Design and Control of a Voice Coil Actuated Robot Arm for Human-Robot Interaction

by

John M. McBean

Submitted to the Department of Mechanical Engineering
on May 7, 2004 in Partial Fulfillment of the
Requirements for the Degree of Master of Science in
Mechanical Engineering

ABSTRACT

The growing field of human-robot interaction (HRI) demands robots that move fluidly, gracefully, compliantly and safely. This thesis describes recent work in the design and evaluation of long-travel voice coil actuators (VCAs) for use in robots intended for interacting with people. The basic advantages and shortcomings of electromagnetic actuators are discussed and evaluated in the context of human-robot interaction, and are compared to alternative actuation technologies. Voice coil actuators have been chosen for their controllability, ease of implementation, geometry, compliance, biomimetic actuation characteristics, safety, quietness, and high power density. Several VCAs were designed, constructed, and tested, and a 4 Degree of Freedom (DOF) robotic arm was built as a test platform for the actuators themselves, and the control systems used to drive them. Several control systems were developed and implemented that, when used with the actuators, enable smooth, fast, life-like motion.

Thesis Supervisor: Cynthia Breazeal
Title: Assistant Professor of Media Arts and Sciences

ACKNOWLEDGEMENTS

My thesis is dedicated to my family. Thanks for the support and inspiration. Thanks for pushing me just hard enough. Thanks for the encouragement, and for the selfless enthusiasm. I am a fortunate son. And a grateful one.

Cynthia, it has been a pleasure working with you. Thank you for giving me such a perfect research opportunity, with the freedom to pursue a new idea, and the trust that it had potential. My graduate career could not have been better. And congratulations on your newest family member. I wish you all the best!

Woodie Flowers, the past several years would have been very different had we not started arguing about catapults 3 years ago. I'm terribly lucky to have gotten in your way by convincing you that I was a liability. Thanks for asking tough questions, and giving credit to my answers. I have learned so much from you.

Fred Cote in the Edgerton Center Machine Shop. While I owe it to you, it would be an insult to say thanks just for the machining education. I thank you for making it fun, keeping me on my toes, entertaining me, and teaching me about more important things than machining. It has been enlightening.

Thank you Leslie Regan for all of your help in pulling this together.

Thanks to all of my friends, the reasons why I've had so much trouble leaving this place.

This research is the work of the Robotic Life Group and the MIT Media Laboratory. The work is funded by the Digital Life and Things That Think consortia.

OUTLINE

LIST OF FIGURES

LIST OF TABLES

CHAPTER 1. INTRODUCTION

The field of robotics is growing rapidly, and its demands are widespread. Robotic systems are typically comprised of mechanical hardware, electrical hardware, sensors, actuators, and computers. In a myriad of different applications, robots sense information about their own state as well as their environment, process that information, and act within their environment to accomplish a goal. The diverse environments in which different types of robots operate impose widely varying requirements in terms of the quality, speed, accuracy, robustness and type of sensing, actuation and processing employed. Consequently, the selection of appropriate sensing, actuation, and processing technology for a robot is generally environment and application dependent. This thesis investigates the selection of an actuator technology that pertains specifically to robots designed to operate in environments where their primary goals involve interaction with people. In the ideal case of a robot as a collaborator with a person, there must be an effective information exchange between the person and the robot, as well as the effective execution of the task at hand (if the task consists of something more than the interaction itself). To fulfill these expectations, it is important for a robot to be able to convey and perceive visual, auditory and tactile information, as well as to interact with and affect its environment. This thesis addresses the implications of these requirements on the design, selection and control of robotic actuators.

Since robots find use in areas ranging from microscopic-scale precision assembly to dinosaur-sized amusement park monsters, there are nearly as many metrics for evaluating actuator technologies as there are applications for them. Some typical metrics for comparing robotic actuators are: strength, response speed, accuracy, robustness to environmental conditions, durability (number of cycles to failure), mass, size, ease of implementation, cost, controllability, sound, stiffness, form factor, safety and scalability [2]. Currently, the majority of robots in operation are used in industrial environments. Spray painting, welding, and pick and place assembly are examples of typical robot applications. As such, the consideration of the interaction between robots and humans (if considered at all) is generally limited to safety and ease of control of the robot by the operator. Further, the actuator selection parameters are very different from those considered for human-friendly, collaborative robots.

The actuator criteria imposed by robots intended for meaningful and useful interaction with humans differ significantly from those imposed by industrial robots. Our primary concern for such robotic actuators is quality of motion. For a rich and effective human-robot interaction, robots must move smoothly, fluidly, and quietly. The motion must be fast enough to make the interaction or the task execution unencumbering and practical, while maintaining a slow enough pace that the human can keep up. The motion must be compliant enough that physical contact between the human and the robot is not dangerous or uncomfortable. Further, it may be important that the human be able to physically guide the robot (in teaching the robot a task or a motion, for example), in which case the robot's motion must be controllable in such a way that it is aware of, robust to, and sympathetic to the touch of a person. This calls for actuators with low mechanical impedances and variable stiffnesses that are readily force-controlled. For certain applications it may also be important that the motion be convincingly organic, as the rigid, precise motion of an industrial robot may not be desirable in a robot intended as

an entertaining companion for a human. In the case of robots of human or mammalian form, the geometry of the actuators may also play an important role in their selection. If the physical appearance, as well as the quality of motion, is to be convincingly organic, actuators must be designed with sizes and shapes that fit seamlessly into organic forms.

Comparisons of robot actuator technologies typically reveal the appealing high power densities of electromagnetic actuators, and the high pressures of hydraulic, piezoelectric, shape memory alloy (SMA), and certain electro-active polymer (EAP) actuators [1]. The conventional metrics of comparison for these actuators tend not to clearly identify which technologies are most suitable for high degree of freedom robots intended for tactile interaction with people. Such comparisons also tend to be misleading in that they may overlook some of the bulky infrastructure required for the implementation of the actuators. Hydraulic actuators, for example, are particularly attractive for their high pressures, low power holding forces, and relatively high speeds. It should not be overlooked, however, that hydraulic actuators are conventionally messy, high maintenance, very stiff, and require large amounts of material overhead for pumps, fluid lines, valves, accumulators and the like. In the selection and development of an appropriate actuation technology for interactive robots, we have considered conventional metrics of comparison (pressure, power density, and controllability), while giving careful attention to the actuator demands that are specific to the field of human-robot interaction (HRI). In short, these demands include quality of motion, quality of tactile interaction, safety, form factor, noise level, robustness to overloading, and ease of implementation and control.

Electromagnetic voice coil actuators (VCAs) show great promise to fulfill many of the aforementioned requirements. They have high power densities, silent operation, smooth, backlash-free motion, variable stiffness, relatively low cost, favorable form factor, and are easily controlled. This thesis covers the design, implementation, control, and evaluation of VCAs as robotic actuators.

1.1 Thesis Outline

We begin in chapter 1 by discussing the requirements imposed on robotic actuators by different fields, and examining the actuator requirements imposed by our specific project within the field of HRI. This serves as the motivation for this thesis. In chapter 2, we discuss the background of robotic actuators, as a means of establishing baselines for comparison across many actuator metrics. We then introduce the work being done on voice coil actuators. We discuss the attributes of voice coil actuators, their advantages and shortcomings (specifically in the context of tactile human-robot interaction), and design parameters that affect their performance. We also describe prior work in the field of VCA technology. In chapter 3, we discuss more specifically the design and construction of our VCAs. We discuss the tradeoffs in VCA design among size, form factor, quality of motion, mass, cost, and controllability. In chapter 4 we describe the implementation of the actuators in a 4 DOF robotic arm to be used in the development of a collaborative robot. In chapter 5, we describe the kinematic and dynamic modeling of the actuators and the arm. Chapter 6 is a discussion of the control system design. We discuss the necessity of an adequate control system to take full advantage of the actuator characteristics, and describe the different methods employed.

In chapter 7 we present the results. We discuss actuator performance, implementation issues, advantages and shortcomings of the mechanical design, compatibility of the components, control system performance, and overall system performance. Finally, in chapter 8, we discuss conclusions and future work. We describe the overall potential of VCAs as viable robotic actuators, as well as potential avenues of research for solving some of the fundamental problems with VCAs. We describe possible developments to ease their implementation and configuration, making them more effective and attractive as replacements for conventional actuators.

1.2 MOTIVATION

The Robotic Life group at the MIT media lab works on developing robots that are socially, intellectually, and physically capable of interacting and collaborating with humans. Currently, the robot used for the implementation and evaluation of the research is Leonardo, a 66 degree of freedom expressive robot that stands approximately 70 centimeters tall. As can be seen in figure 1.1, Leonardo has a mammalian form factor, with a skeletal and muscular structure resembling that of a small child. He is a non-mobile robot, with the majority of his actuators located on his body. The larger actuators are located in the box on which Leonardo stands, and drive the joints via cables or linkages. All of Leonardo's actuators are brushed DC motors with gearboxes, using potentiometers and magnetic encoders for position and velocity feedback.

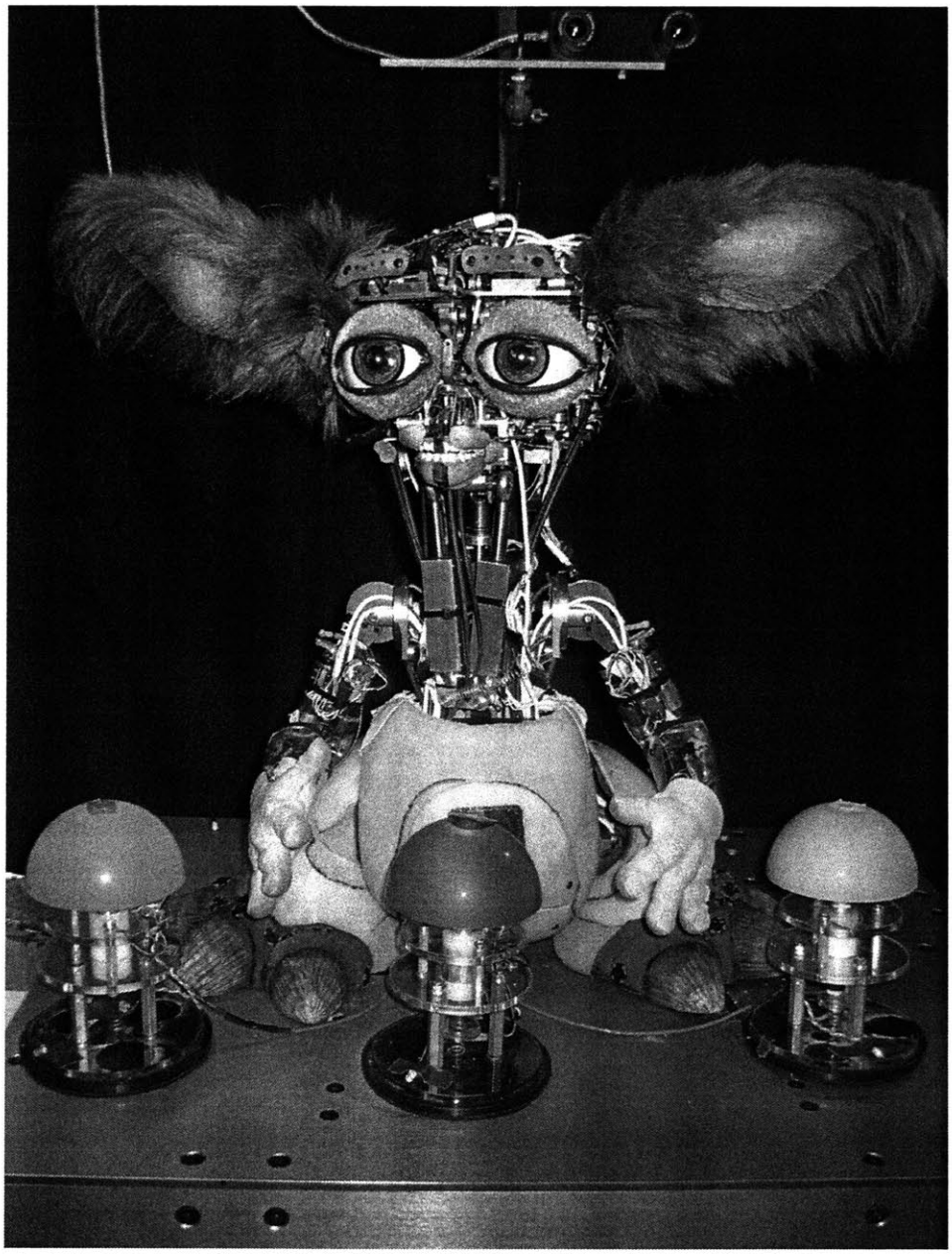

Figure 1.1 Robotic Life Group's robot, Leonardo

Figure 1.2 Leonardo with his fur

DC motors have high volumetric power densities and low output torques.[1] As a result, DC motors may be significantly smaller than human muscles to achieve similar power outputs for a given joint. However, these high power outputs are achieved at high speeds and low forces, necessitating large transmission ratios to attain the torques demanded by robotic applications. Unfortunately, the use of such transmissions usually implies the introduction of backlash, noise, bulk, mass, excessive stiffness, torque ripple, and susceptibility to breakage. The peak torques achievable in small scale robotic applications (like Leo) are generally limited by the strength and robustness of the materials used in the gear train, rather than the ability of the motor to transform electrical power into mechanical power. Such is the case with Leonardo's actuators. Most of Leonardo's actuators have gear trains (see figure 1.3) with high ratios so that his joints are effectively infinitely stiff (non-backdriveable) as viewed from his workspace.

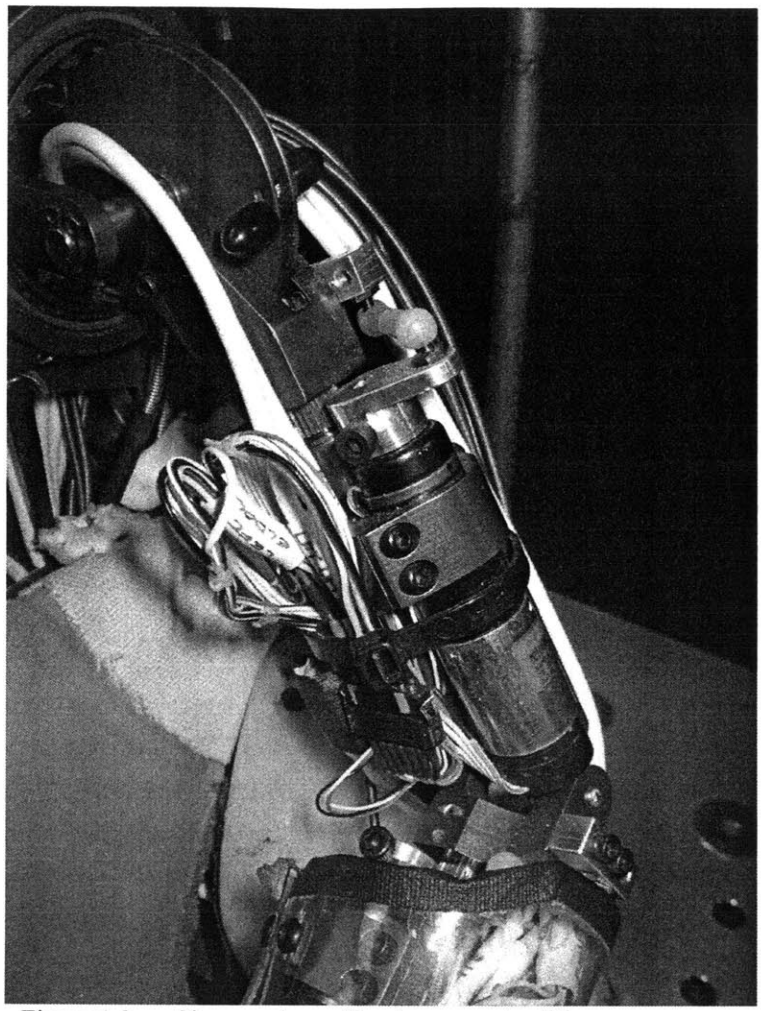

Figure 1.3 Closeup view of Leo's gearmotor-driven upper arm

The implication is that smooth, safe contact between Leo and his environment (people and objects) is difficult at best. Fluid, jitter-free motions at human-scale velocities and accelerations are unachievable. Sudden forces exerted on Leo by people or objects in his environment result in damage to his joints or his actuators. Tactile interactions with Leo are rigid, unforgiving, and slow.

There is an obvious need for an improvement in the actuators used in robots such as Leo, if they are to convey and interpret information effectively and exhibit a life-like presence. Table 1.1 presents the general functional requirements that we have chosen as being the most important in the development of actuators for a collaborative HRI robot. The table lists specific actuator characteristics that will be necessary to achieve the functional requirements.

Table 1.1 ACTUATOR FUNCTIONAL REQUIREMENTS AND CORRESPONDING CHARACTERISTICS

Functional Requirement	**Actuator Characteristics**
High Quality of Motion	-low backlash -low coulombic friction/stiction -low mechanical impedance -moderate accelerations attainable -inherent damping
High Quality of Tactile Interaction	-variable stiffness -force or impedance controlled -adequate strength
Safety	-high permissible control system gains -low inertia -high compliance -force or impedance sensing means
Organic form factor	-moderate power and force density (to minimize actuator size) -bilateral, push/pull actuation (to eliminate necessity of opposed pairs) -linear, as opposed to rotary actuators (to mimic muscle) -small or no mechanical transmissions (minimize bulk)
Quiet operation	-few moving parts -low or no transmission ratios (eliminate high speed mechanical contact)
Robustness to overloading	-few mechanical parts. -backdriveable -high compliance
Easy to implement and control	-minimize need for complex gear trains to change the actuation direction -use readily available materials -low hysteresis

1.3 THESIS SCOPE

Leo needs new actuators. The goal of this thesis was to research, design and construct voice coil actuators that will serve as viable replacements for the conventional actuators used in robots such as Leo. We have designed and built a 4 degree of freedom arm as an evaluation platform for the new actuators, and as a potential model arm for the next generation of Leonardo. We also developed and evaluated control systems that exploit the actuators' favorable characteristics to improve robot performance in the areas where Leo is deficient.

CHAPTER 2. BACKGROUND

2.1 Robotic Actuator History

In this section we give an overview of the state of the art of robot actuator technology. A comprehensive comparison of actuator technologies was published by Hollerbach, Hunter, and Ballantyne in 1992 [1] and is still very much relevant today. The vast majority of actuators used in robotic systems to date employ one or more of the technologies described in that paper. Many of these technologies have been proven to be robust, cheap, and readily available. Under a paradigm where robots are expected to be bulky, dangerous, rigid, precise, and serve strictly industrial applications, many of these conventional technologies excel. A recent push for biologically-inspired robots that interact directly with humans has spurred much research in artificial muscles. Many of these younger, biomimetic materials-based actuation technologies are beginning to provide competition for conventional technologies as robotic actuators [2], [3], [7].

First, we will define some terms that will be used in the discussion of the different actuation technologies. *Power density* is the amount of mechanical power output an actuator can produce, normalized by its mass or volume. *Mass power density is measured in* Watts per kilogram; *Volume power density* is measured in Watts per cubic meter. *Peak pressure* is the maximum force an actuator can produce, divided by the cross-sectional area of the actuator. *Pressure density* is the peak pressure attainable by the actuator, normalized by its mass or volume. *Maximum strain* is the maximum percentage by which the actuator can change its length while producing a force. *Efficiency* refers to the overall energy conversion efficiency – the mechanical output power of the actuator divided by the power input to the actuator (electrical, chemical, or thermal). Finally, *work density* is the amount of work generated over one full cycle of an actuator, divided by the actuator mass.

The following table comprises a combination of our own work and research, as well as that of Madden, Hollerbach, Hunter, and Ballantyne [1], [2]. Attempts to make fair comparisons of actuator technologies can be misleading, as universal metrics for evaluating performance are difficult to find, and often do not take into full account all of the components of the actuators. For example, note that no units have been chosen for the comparison of the speeds of the different types of actuators. This is because a rigorous experiment has not been conducted where each of the actuators is subjected to a comparable speed or frequency response test; hence the speeds of the actuators are loosely characterized and described in the table. Other examples of the potentially misleading nature of actuator comparisons are the apparent high pressure and power densities of hydraulic and pneumatic actuators. Conventionally, this evaluation neglects the mass of the material overhead (pumps, valves, fluid lines, etc). This is acceptable only for very high DOF robots, where the mass and volume of the material overhead is in fact small compared to the overall mass of the system). We have attempted to highlight, where possible, such ambiguities in actuator comparison. Further, we have made attempts to describe the actuator characteristics that are especially relevant to HRI robot design.

Table 2.1 ACTUATOR SYNOPSIS

Technology	Description
Mammalian Muscle	Moderate peak stress (0.35 MPa) Moderate strain (20%) Moderate power density (50W/Kg) High (and variable) compliance Flexible form factor Produces smooth, fluid motion Low material overhead Low-moderate pressure density Moderate speeds Unilateral (Pull-only) actuation Inefficient at zero-velocity (holding) forces.
Electromagnetic (VCAs)	Low peak stress (0.05-0.1 MPa) Large strain (50%) High power density (200 W/Kg) Efficiency varies from high (~90%) at high speeds and short strokes to low (~5%) at low speeds and high stroke lengths Fast High compliance Form factor compatible with human-form design Produce smooth, backlash-free, quiet motion Low material overhead. Few moving parts; robust to overloading Bi-directional (push-pull) actuation High force applications require mechanical transformers
Hydraulic	High peak stress (20 MPa) Large strain (50%) High power density (600 W/Kg) (difficult to account for material overhead mass, and extremely high instantaneous power delivery) High stiffness Very high material overhead (valves, lines, pump, accumulator, filters, etc) High maintenance Bilateral actuation Moderate-high speeds (although inefficient at high speeds)
Pneumatic	Moderate peak stress (0.7 MPa) Large strain (50%) High power density (200 W/Kg) (difficult to account for material overhead mass, and extremely high instantaneous power delivery) High efficiency (~90%) Fast, but with moderate settling times due to compressible gas and

Pneuamatic (cont'd)	control difficulty. Moderate compliance High material overhead Bilateral actuation Often loud
Piezoelectric	High peak stress (35 MPa) Low strain (1%) Very low power density (0.1 W/Kg) Very high speeds (high frequency, very short stroke actuators – less practical for robotic applications) Moderate material (and control) overhead Must be driven with high voltages Quiet Bilateral actuation "Inchworm" and "Waverotor"- type actuators have been developed with larger strains and lower stresses
Magnetostrictive	High peak stress (10 MPa) Low strain (2%) Very high power density (5 W/Kg) High efficiency (~80%) High speeds are possible Usually unilateral actuation High material overhead (bulky magnets or coils are required for activation)
NiTi Shape-Memory Alloy (Thermal)	Very high peak stress (200 MPa) Low strain (1-8%) Very high power density (100kW/kg) Very low efficiency (<5%) Very difficult to control Slow Low voltage activation Low cycle life Unilateral actuation Can have good form factor for mammal-form robots
Dielectric Elastomers	Moderate-high stress (1-10 MPa peak) Moderate-large strains (20%-380%) Moderate efficiency (15%-90%) Fast Require high voltages Unilateral actuation High material overhead (Pre-stretching mechanisms required)
Relaxor or Ferroelectric Polymers	High stress (45 MPa) Low strain (<7%) High work density (<1MJ/m^3) High stiffness

Relaxor or Ferroelectric Polymers (cont'd)	Exhibits hysteresis High driving voltages (>1kV) Unilateral actuation Large material overhead (power supply, control electronics)
Liquid Crystal Polymers	Low-moderate stress (0.01-0.45 MPa) Moderate-high strains (2%-45%, depending on whether thermal or field induced strain) Moderate-high efficiency Difficult to control (creep) New material High driving voltages Slow
Conducting Polymers	High stress (5-34 MPa) Low strain (2%) High stiffness Low driving voltage (~2V) High work density (100kJ/m^3) Slow Bilateral actuation Low efficiency
Molecular Actuators	Moderate-high stress (>1 MPa) Moderate-large strain (20%) High work density (100kJ/m^3) Low driving voltage (~2V) Slow Unilateral actuation New technology
Carbon Nanotubes	High stress (>10MPa) Very small strain (0.2%) Low driving voltage (~2V) Inefficient Unilateral actuation Expensive
Ionic Polymer Metal Composites (IPMC)	Large strain Low driving voltage (<10V) Unilateral actuation Low efficiency
Ferromagnetic Shape Memory Alloys	High stress (<9 MPa) Small strain (<10%) Fast High efficiency Unilateral actuation High material overhead (field magnets)

2.2 Voice Coil Actuator Technology and Prior Work

Voice coil actuators have been around for decades. They have been used primarily as the sources of force in audio loudspeakers, and as drive mechanisms for disk drive read heads. As described in Section 2.1, they are characterized by high power densities, high bandwidths, and relatively low pressures. A voice coil (see figure 2.1) is an electromagnetic actuator that generally consists of one or more coils of wire placed in a magnetic field, such that there is a force is produced when current flows in the coil. The voice coils discussed in this thesis use permanent magnets as the magnetic field source.

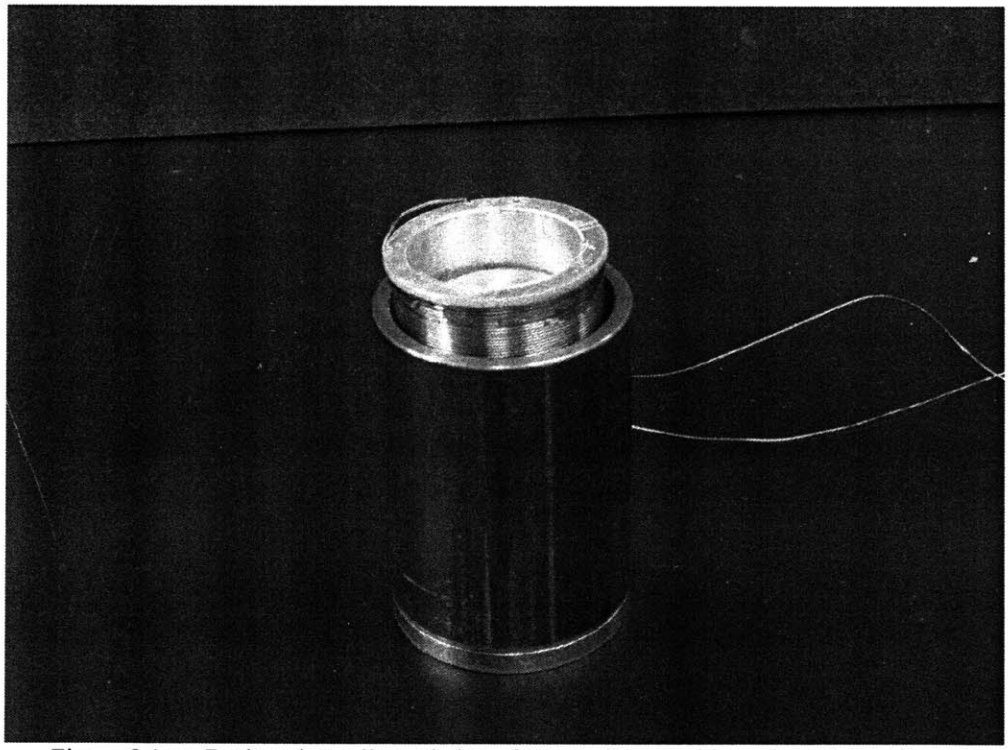

Figure 2.1 Basic voice coil consisting of magnetic assembly and moving coil

The force produced by the actuator (the voice coils described in this thesis are linear, rather than rotary actuators) is given by:

$$F = n\pi diBSin\theta \; ; \qquad (1)$$

where n is the total number of coils of wire, d is the average diameter of the coil, i is the current in the wire, B is the magnetic field strength, and ? is the angle between the magnetic flux lines and the direction of the current. The part of the actuator that moves,

and to which the load is attached is generally called the *rotor*, and the stationary part (in this case, the part which houses the coils) is called the *stator*.

Focus areas for improving the force outputs of VCAs are evident from (1). Square wire has been used to increase coil winding density (increasing n for a given volume). Attempts to increase the currents thermally permissible in the coils include development of low resistance coil materials, use of active cooling techniques [1], and the use of ferromagnetic fluid suspended in the air gap between the coil and the magnet. Since heat adversely affects that magnetic field strength of permanent magnets (especially NdFeB), the benefits of increased heat dissipation are twofold. Much work has been done to increase the magnetic field strength across the air gap. Permanent magnet materials, such as NdFeB, with higher magnetic remanences and higher temperature tolerances have been developed. Actuator geometries have been refined so as to "focus" the flux in the air gap and minimize leakage [5]. The use of ferromagnetic fluid also increases the field strength and uniformity, but its effects are limited due to its low magnetic saturation. The preceding techniques have been shown to greatly improve VCA performance. In the construction of these prototype actuators, however, we have opted for a simple design, leaving room for the implementation of such techniques in future revisions.

Voice coils are typically not commutated, meaning the entire coil becomes energized when a voltage is applied. This represents a source of inefficiency for voice coils, as waste heat is produced even in the coils that are not contributing significantly to the force produced by the actuator. For this reason, VCAs with arbitrarily long strains are not practical.

2.2.2 Voice Coil Actuators for Human-Robot Interaction

For their application to HRI and force-controlled robots, VCAs have many advantages over other forms of actuation [5],[6], [10]. The major advantages of electromagnetic actuators are their speed, smooth motion, silent operation, high efficiencies, ease of implementation, and robustness to overloading. If, for example, a directly-driven VCA is pushed against the direction of its force, it will simply continue to apply a force proportional to its current, and allow itself to be backdriven if the force exceeds that value. Power input to the actuator in the form of current is then dissipated as heat. This fundamental property of VCAs (and all backdriveable actuators) is a key safety advantage for robots intended to touch, and be touched by, people. VCAs tend to have only one moving part, with only two points of contact (bearings at either end). This makes for an actuator with low wear, long life, quiet operation, and excellent shock loading tolerance.

Another major advantage that VCAs have over mammalian muscle, and other forms of actuation that imitate it closely, is that VCAs are bilateral actuators, meaning they can push or pull with comparable force. This eliminates the cumbersome, bulky, and often difficult to control need for bilaterally opposed pairs of actuators at every joint. Effectively, the *power density* of VCAs ought to be compared to *half* that of unilateral actuators, when they are being considered as sources of force for robotic joints which will undergo flexion and extension. If we consider the metric of *Pressure density*, bilateral

actuators (such as VCAs) have a twofold advantage over their unilateral counterparts (such as muscle).

For high force applications, mechanical transformers (gear reductions, for example) are needed to transform the power delivered by electromagnetic actuators from high speed/low force to high force/low speed. Mechanical transformers usually introduce backlash, noise, stiffness, and control problems. They also decrease robustness and increase maintenance requirements. This, of course, is the fundamental problem with VCAs, and necessitates that direct-drive robots using VCAs use larger actuators than might be necessary if a different actuation technology were chosen, or if mechanical transmissions were used. Due to their high power densities, electromagnetic actuators sized to achieve a certain force for an application will be found to have higher power outputs than required for the application. This mismatching of peak power and peak pressure (where mechanical transformers, or geartrains are not used), is discussed further in chapter 8. Our VCAs have demonstrated sufficient pressures to be free of the need for mechanical transformers of any kind, for use in non-mobile, low-payload HRI robots comparable in size, shape and strength to humans.

While rotary electromagnetic actuators (brushed or brushless DC motors, for example) have similar performance characteristics to VCAs, they have a distinct geometric disadvantage when compared to VCAs, for use in human-form robots. VCAs have a similar form factor to human muscle – they can have large length/diameter ratios (meshing symbiotically with limbs of mammalian-form robots); they can have comparatively high strains; they are linear actuators, and can therefore be implemented in ways that look and behave like mammalian muscles without the use of bulky, heavy, or complex drivetrains. Rotary actuators, on the other hand, would have to be oriented parallel (preferably concentric) with the axis of the joint, and in order to occupy the same volume as a corresponding VCA, would have to have a diameter or length that would extend far beyond the envelope of the form factor of a human limb. Further, if the rotary actuator should be oriented in a more geometrically favorable way, a drivetrain may be necessary to transmit the mechanical power from the actuator to the joint axis. Such drivetrains introduce backlash, noise, jitter, stiffness, and control problems, while increasing system mass, volume, and susceptibility to breakage.

The low peak pressures produced by VCAs (approx. a factor of 4 lower than that of human muscle, for short durations) require that the actuators be oversized in comparison to muscle, and are weaker than a muscle of similar size. Consequently, the arm that is the subject of this thesis is approximately the size of that of a young child, and has strength performance that ranges from significantly weaker than a child (for short durations) to comparable strength to a child (for longer durations) [8]. Since many HRI robots may find their applications in areas that do not require high payloads, high contact forces, or high inertial forces, the compromise between decreased strength and smooth, quiet, backlash-free, fast, easily-controlled motion seems acceptable.

CHAPTER 3. VOICE COIL ACTUATOR DESIGN

3.1 Detailed Description of VCA Design

We have experimented a variety of VCA designs. Figure 3.1 shows a moving – coil design with a square cross section.

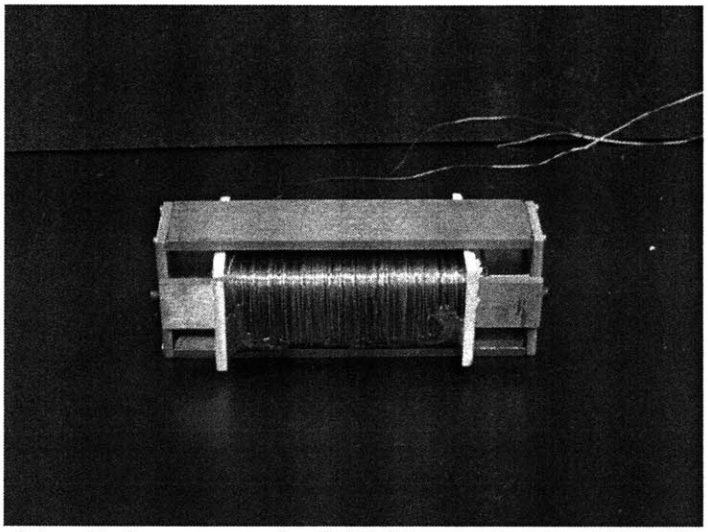

Figure 3.1 Early prototype of radial field, square cross-section voice coil

The stator, consisting of NdFeB permanent magnets is constructed such that there is a uniform magnetic flux oriented from the inside (axis) of the actuator to the outside. It is a 2-dimensional approximation of a radial magnetic field. This design has the feature that strains of significantly greater than 50% can be achieved, but at correspondingly lower pressures than other designs would afford. Figure 3.2 shows a sectional view of a possible embodiment of a radially magnetized voice coil design. The white arrows represent the magnetic flux lines.

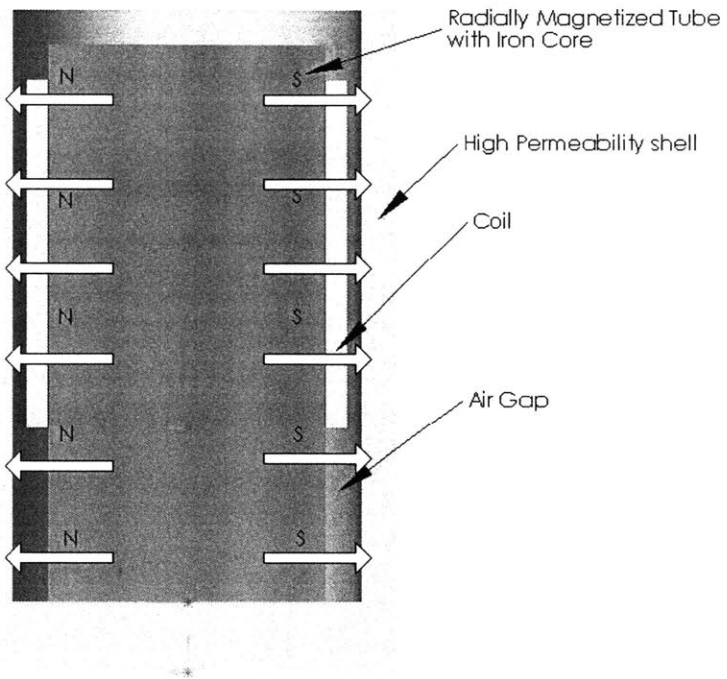

Figure 3.2 Solid model of radial voice coil.

A radially magnetized tube with an iron core, concentric with an iron shell establishes a magnetic field across the air gap. A major advantage to radial designs is the uniformity of the field strength achievable along the length of the actuator. The cost, however, is that it is difficult to radially magnetize permanent magnet materials, making them expensive, and causing their field strengths to be typically 10-20% lower than axially magnetized magnets of the same material. Figure 3.3 shows an axially magnetized design, where, similarly to the radial design, the magnetic flux runs along the axis of the magnetic core, into the iron shell at one end of the actuator, and then back across the airgap to the core, to complete the magnetic circuit. The white arrows represent the magnetic flux lines.

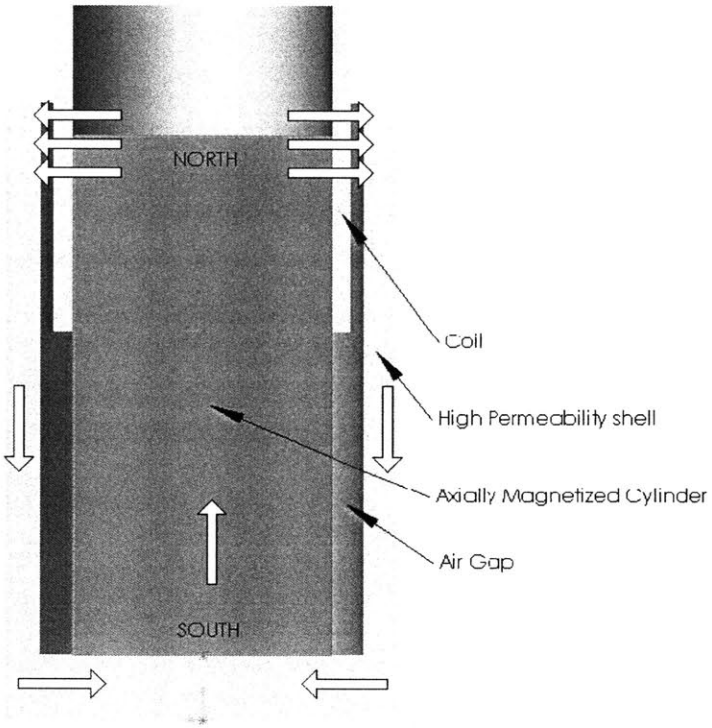

Figure 3.3 Solid model of axial voice coil.

The major difference between axial and radial designs is the uniformity of the flux in the air gap, along the length of the actuator. While radial designs achieve relatively uniform field strengths, axial designs tend to concentrate the flux near the open end of the air gap. Just as an axially magnetized permanent magnet behaves in air, the radial component of the flux is concentrated at the ends, not along the length, of the magnet. The axially magnetized, moving coil VCA in figure 3.3 is a typical design and is commercially available.

We have chosen a moving-magnet design, as opposed to moving coil design for the VCAs to be used in the arm. While a moving-magnet design can result in a slightly greater moving mass (this, of course, is not always the case and depends on the coil mass and whether the VCA is being designed for high force or high speed operation), it affords a simpler construction geometry enabling smaller, more streamlined actuators. A sectional view of the wrist actuator can be seen in figure 3.4.

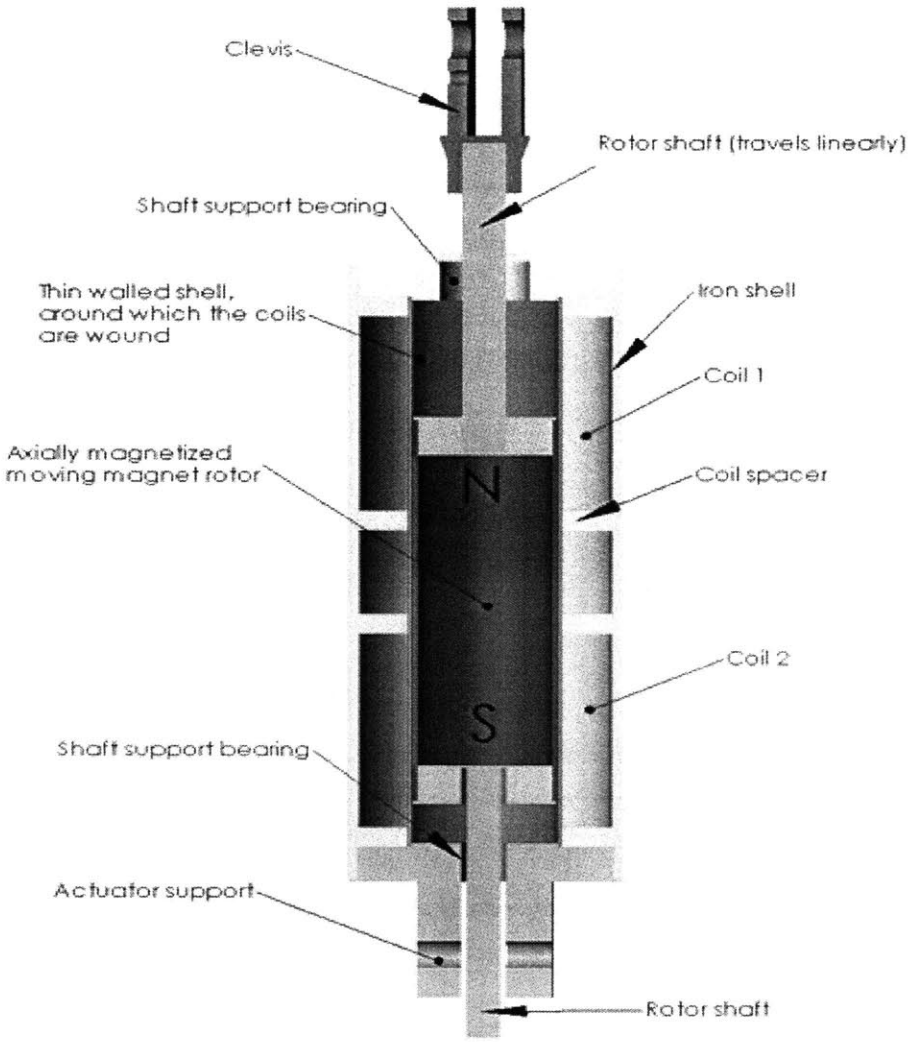

Figure 3.4 Sectional view of the moving-magnet, axial VCA used in the wrist

The stator consists of two independently wound coils inside a thin iron shell. The rotor is a cylindrical, axially magnetized NdFeB permanent magnet, with shafts extending from each pole, supported at the ends in linear bearings. The lengths of the rotor and the coils are designed such that throughout the range of motion of the actuator, one coil remains in the magnetic field of the south pole of the rotor; the other coil, the north. The current in each of the two coils is in opposite directions, matching the opposing polarities of the magnetic fields at either end of the rotor. The strokes of the bicep and wrist actuators are 4.7 cm and 2.5 cm, respectively. Figure 3.5 shows the finished bicep and forearm actuators.

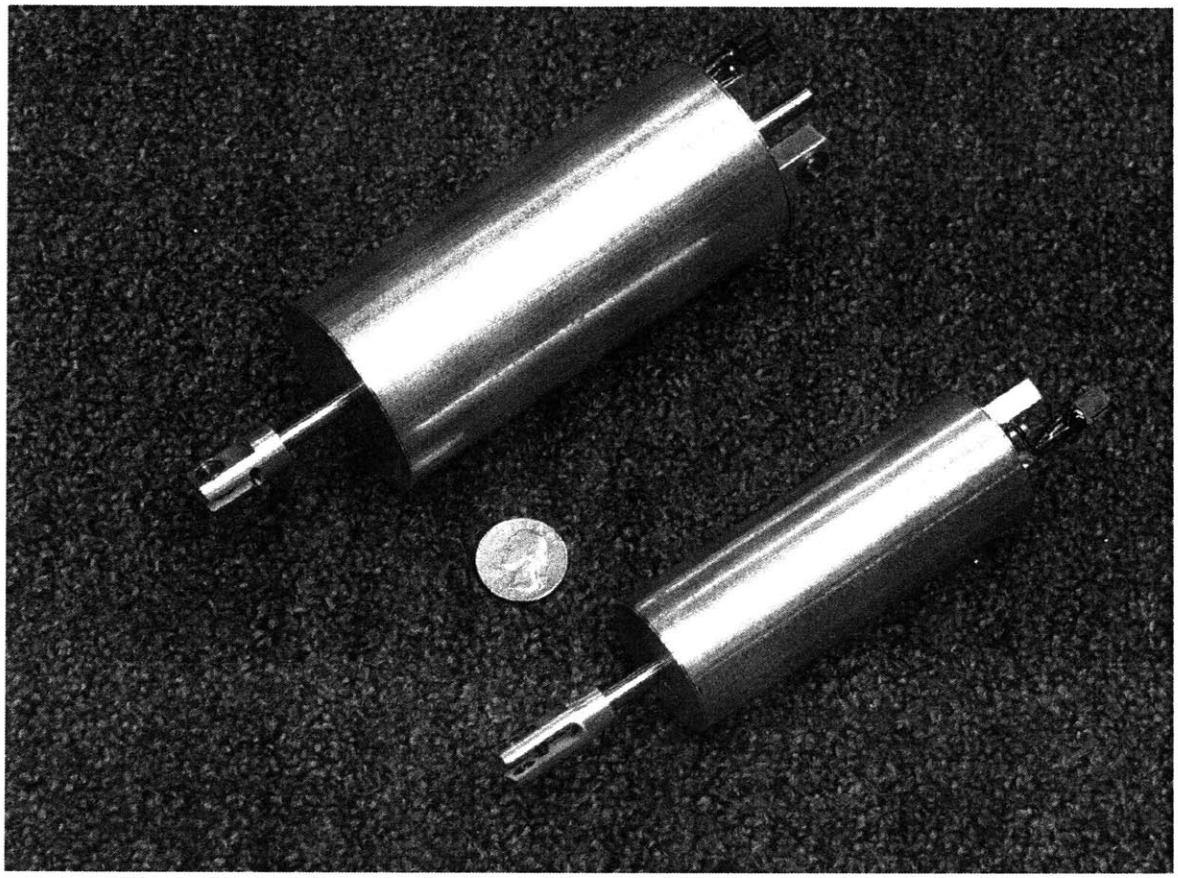

Figure 3.5 Bicep and forearm voice coil actuators

3.2 SPECIFICATIONS

End effector forces of 20 N were desired on the arm, which correspond to peak actuator forces of approximately 100 N and 50 N for the bicep and forearm actuators, respectively. Table 3.1 shows the parameters for each actuator design, based on assumptions of an average air gap field strength of 0.25 T, and magnetic field perpendicular to the actuator coils.

Table 3.1 ACTUATOR PARAMETERS

	Desired Peak Force (F)	**Peak Current (I)**	**Average Field Strength (B)**	**Average Coil Diameter (d)**	**Number of Coils (n)**
Forearm	50N	3A	0.25T	0.0287m	840
Bicep	100N	3A	0.25T	0.0405m	1352

The permanent magnets used in both the forearm and bicep VCAs are axially magnetized NdFeB (grade N40) rods with surface field strengths of approximately 1.25 T. The most significant unknown in the above table is the average air gap field strength. The flux behavior across the air gap is difficult to measure or model. Consequently, empirical data was collected (tests were done on a BEI voice coil), and conservative estimates were made for the expected average field strength. Given the large degree of uncertainty in this and other estimates, the table above incorporates a safety factor of 2 in terms of peak actuator force.

We have built and tested a variation on this voice coil design (see figure. 3.6). By effectively stacking smaller VCAs within one, and connecting their outputs to a common rotor such that their forces sum in parallel, the limit on peak actuator pressure effectively vanishes. Practical design considerations would of course limit the pressures achievable, but the force produced in the actuator will grow linearly with length, while the diameter stays constant. This of course would make VCAs look more attractive with respect to the metric of peak pressure, once again making it difficult to characterize the actuators in a normalized way such that they can be compared fairly with other technologies. The technique of increasing length for higher force is relevant because it is often the case in designing human-form robots (with limbs having high length/diameter ratios) that adding width, or thickness to the actuators (limbs) is very costly, but longer actuators, as means to higher forces, can be accommodated. A 3-stage prototype of a VCA using this design has been built and has verified the possibility of increasing peak pressure in this manner, but was not used in the construction of the direct-drive arm presented in this thesis.

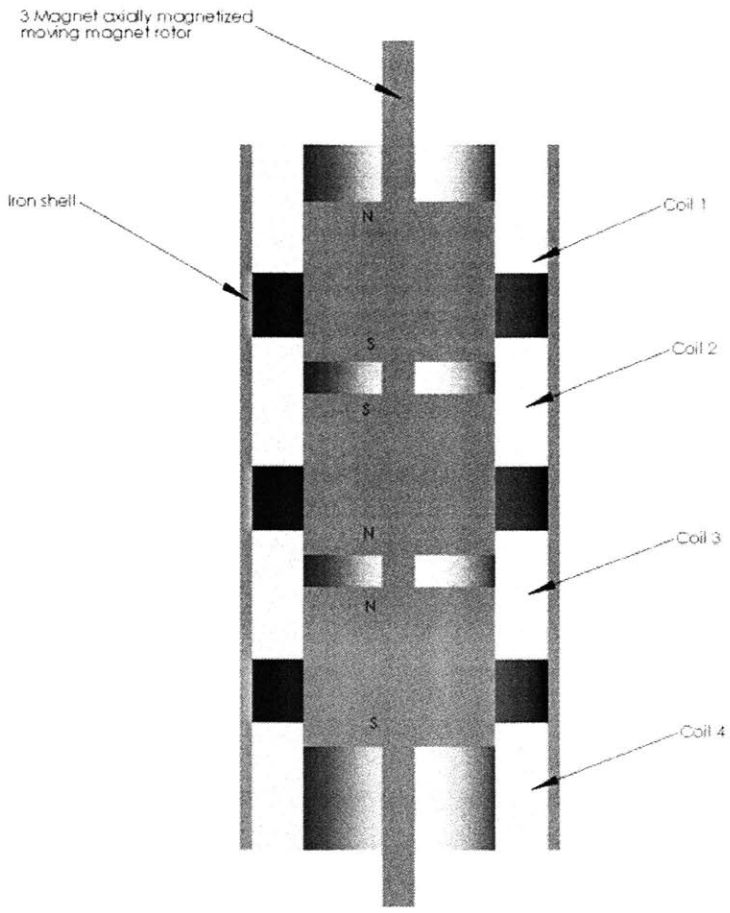

Figure 3.6 Solid model of parallel stacked voice coil actuator

3.2.2 Cost

The VCAs constructed for this thesis use readily available materials. The internal components (the coil separators, the shell around which the coils are wound, the endplates) are machined from aluminum; the shafts are standard hardened steel shafts, running in ceramic linear bearings. The outer shell is thin-walled steel tubing. The assembly of the VCAs is entirely by press fit. As a result, with the exception of some tight tolerance machining operations, the construction and assembly of VCAs is easy, cheap and fast. Because VCAs have fewer moving parts, and do not involve delicate mechanical components such as brushes and commutators, their cost, complexity and manufacture times are lower than those of DC motors. As a result of the simplicity of their design, they are also more robust to operating conditions than DC motors.

3.2.3 *Efficiency*

A major shortcoming of VCAs is their inefficiency at low speeds. Their low backdriveability necessitates that they consume significant amounts of power, even while not moving. This problem can be alleviated to some extent by using springs and carefully choosing the geometry of a robot so as to minimize constant loads, such as gravitational forces. Robot design with voice coil actuators should therefore take inspiration from the way human bodies are designed. Relaxed states should involve low torques by ensuring that joints settle in local equilibria (stable equilibria, in the case of a relaxed shoulder or elbow, or unstable equilibria as in the case of a locked knee in a low-energy standing position). Figure 3.7 shows the measured zero-velocity power consumption by the forearm and bicep actuators, as functions of holding torque.

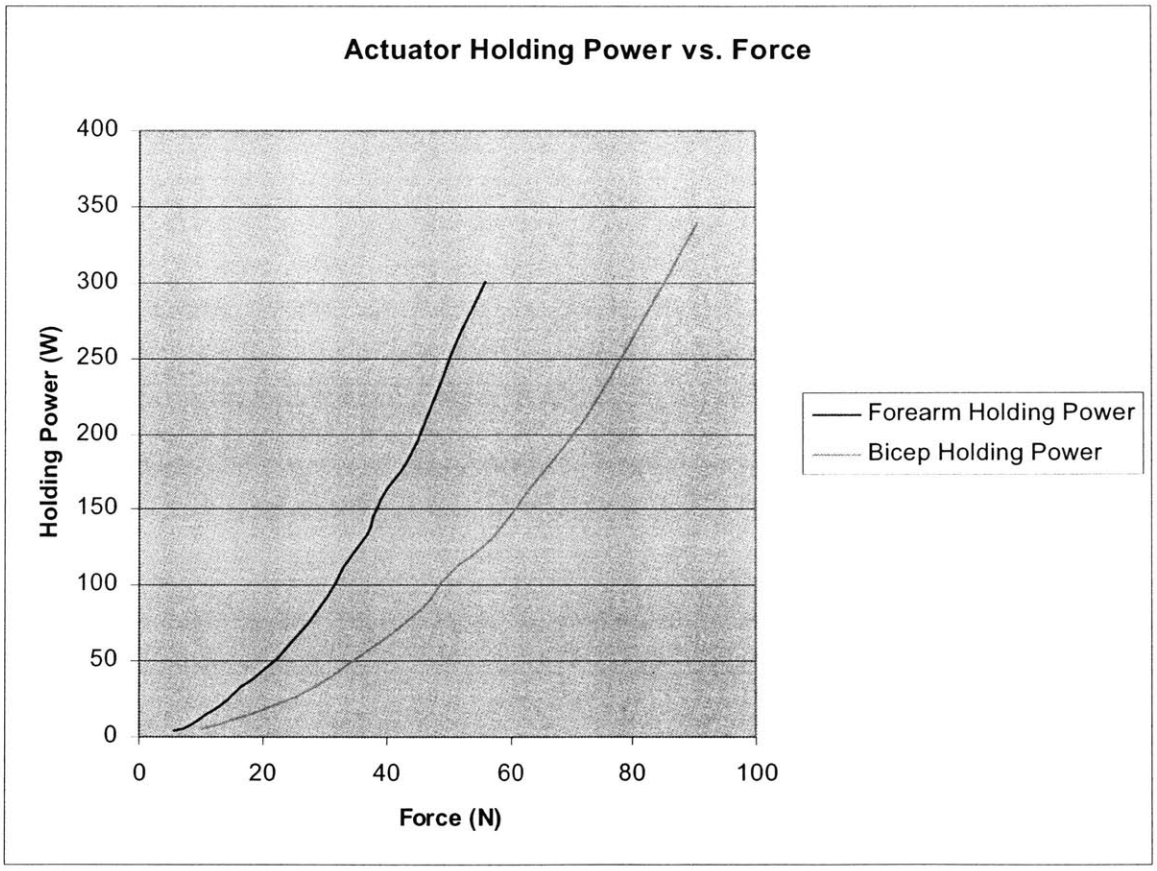

Figure 3.7 Measured zero-velocity holding power for the voice coil actuators

For small, non-mobile robots with low payload capacities, and whose main goals are smooth, friendly interactions with humans, the tradeoff between efficiency and quality of motion is acceptable.

CHAPTER 4. ARM DESIGN

4.1 MECHANICAL DESIGN

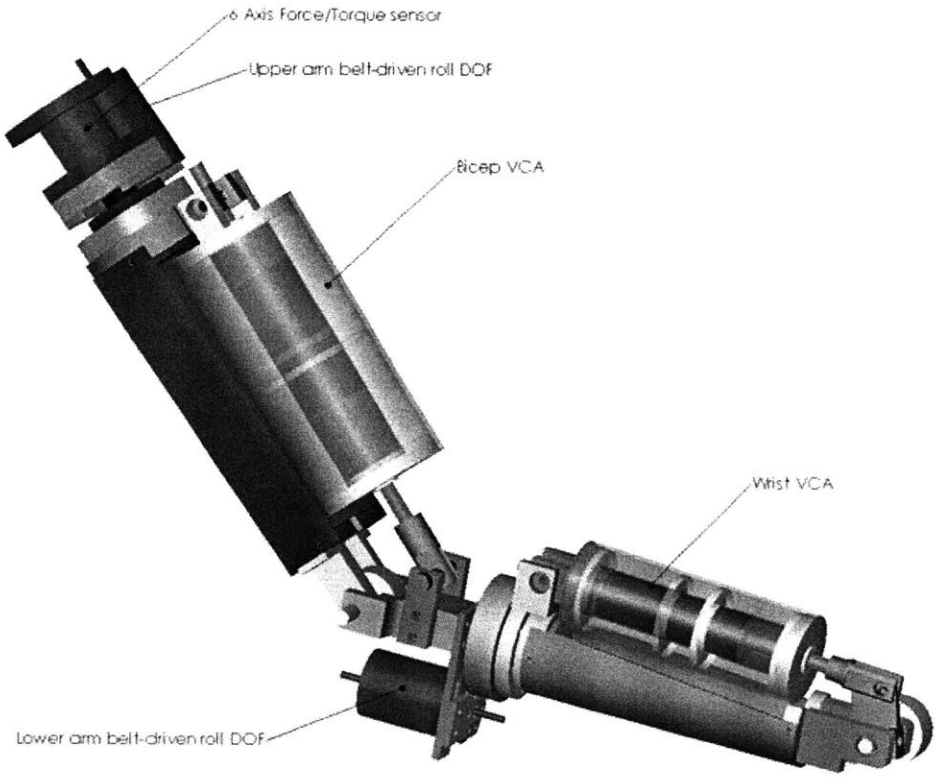

Figure 4.1 Solid model of 4 degree of freedom direct-drive arm

Figure 4.1 is a solid model of the 4DOF direct-drive robotic arm we have built. VCAs drive the bicep and forearm degrees of freedom, while brushed DC motors are driving the upper and lower arm roll degrees of freedom. The roll degrees of freedom are necessary to give the arm enough dexterity to execute meaningful trajectories. The geometry of the arm is modeled after a human, with a forearm slightly longer than the upper arm. The end effector is currently a small knob. This is useful for developing and evaluating the VCA mechanical and control systems, but in the future, hands with tactile feedback may be implemented. The range of motion of the arm is comparable to that of a

human. The elbow and wrist have approximate ranges of motion (ROM) of 90°, while each of the roll degrees of freedom has an ROM of approximately 200°. Table 4.1 summarizes the properties of the arm.

Table 4.1 ARM DESIGN PARAMETERS

Peak End Effector Forces		20N
Peak Acceleration (hand)		2g
Peak Acceleration (forearm)		1g
Joint Ranges of Motion	**Upper arm roll**	200°
	Lower arm roll	200°
	Bicep	90°
	Wrist	90°
Dimensions (lengths)	**Upper arm**	0.20m
	Forearm	0.17m
	Hand	0.08m

The arm is constructed mainly of aluminum. The arm segments (or bone structure) are sections of thin-walled aluminum tubing, to maximize stiffness and minimize weight. All rotational axes use preloaded ball bearings, to ensure that the structure of the arm does not compromise the smooth, muscle-like performance of the actuators. The bearings minimize noise, backlash, and friction. Figure 4.2 shows the method of using a set screw to spread the arms of the actuator clevis to apply an adjustable preload to the clevis bearings.

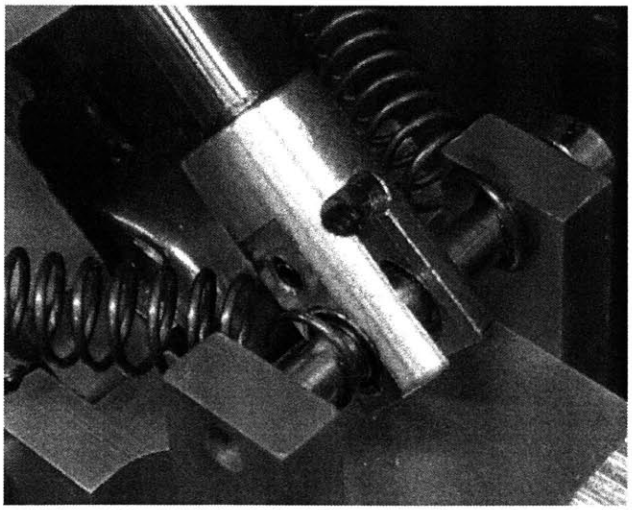

Figure 4.2 Photo of clevis bearing preload technique

The upper arm roll and elbow degrees of freedom have preload springs to help offset the gravitational torques due to the mass of the lower arm segments. The springs are not necessary, but they improve the arm's performance, give it a more natural resting position, and minimize the risk of sudden collisions when the power to the arm is turned off. The elbow springs are shown in figure 4.3.

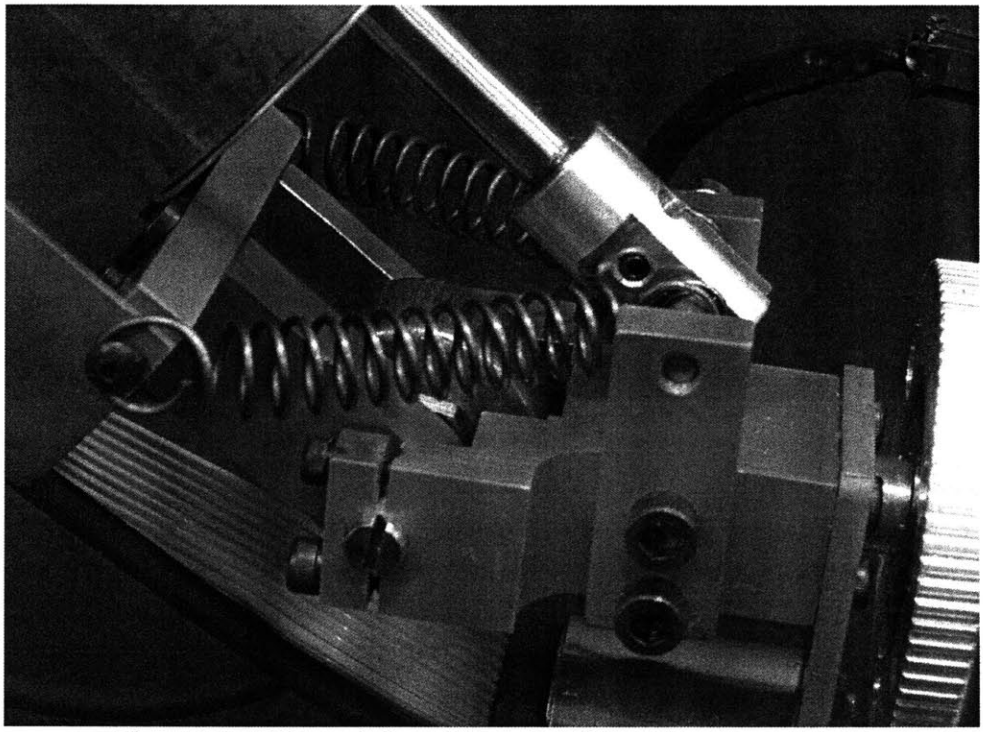

Figure 4.3 Photo of elbow joint springs for gravity compensation

4.2 Actuation and Feedback

The bicep and wrist degrees of freedom are driven by VCAs, and the angular positions of the two joints are obtained via Hall Effect rotary position sensors (Honeywell HRS100). The VCAs attach to the arm segments upon which they act (forearm and hand) at a distance from the joint that is approximately $1/5^{th}$ the length of that segment. End effector forces are therefore approximately $1/5^{th}$ of actuator forces. The upper and lower arm roll degrees of freedom are driven by Maxon Motors brushed DC motors. The motors act on the roll segments of each arm via a 8:1 belt reduction. The reduction allows for a moderate increase in torque, while maintaining a very high degree of backdriveability, and minimizing problems associated with gearboxes. The belts introduce no backlash, and they have some inherent damping that helps in the control of the joint positions. Joint position and velocity information for the two roll degrees of freedom are obtained via Maxon MR encoders on the backs of the roll motors.

For future control system development on the arm, there is a 6 axis force/torque sensor in series with the upper arm, that will be used to measure inertial forces, as well as gravitational forces (for future implementation of trajectory, force, impedance, or hybrid control schemes). Local force sensors (closer to the end-effector) could be used to form force-control loops around contact and payload forces. A potential future development for VCAs is to include integrated position, velocity, and force sensors in the actuators themselves.

4.3 Electrical and Control Hardware

The control system development for the arm was done on an IBM workstation, using the DSP-based DSPACE prototyping hardware and software. The DSPACE software interfaces with Matlab's Simulink program, and the hardware interfaces with the sensors and actuators via a 8 channel ADC and a 8 channel DAC. All control system software was developed and implemented using Matlab and Simulink. The amplifiers used to drive the roll motors and the wrist VCA (the less powerful of the two VCAs) are Maxon Motors linear amplifiers with peak current outputs of 2 Amps. The elbow VCA is driven by a higher power Maxon Motors pulse width modulation-based controller with a peak current output of 10 Amps. The opposing pairs of coils in each VCA are driven by the same control signal, in opposite directions. Figure 4.4 shows the motor driver setup, consisting of linear amplifiers, digital amplifier, and Dspace I/O board, used to drive the arm.

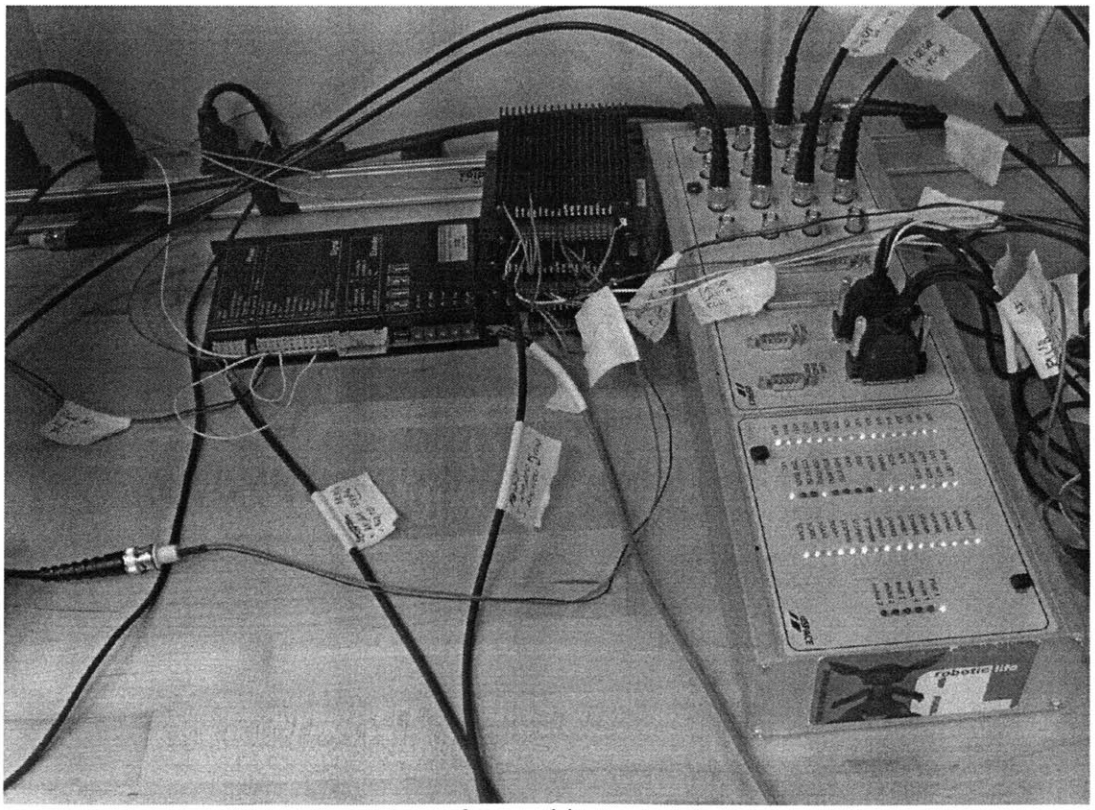

Figure 4.4 Photo of motor drivers and control hardware

Finally, a photograph of the finished arm can be seen in figure 4.5.

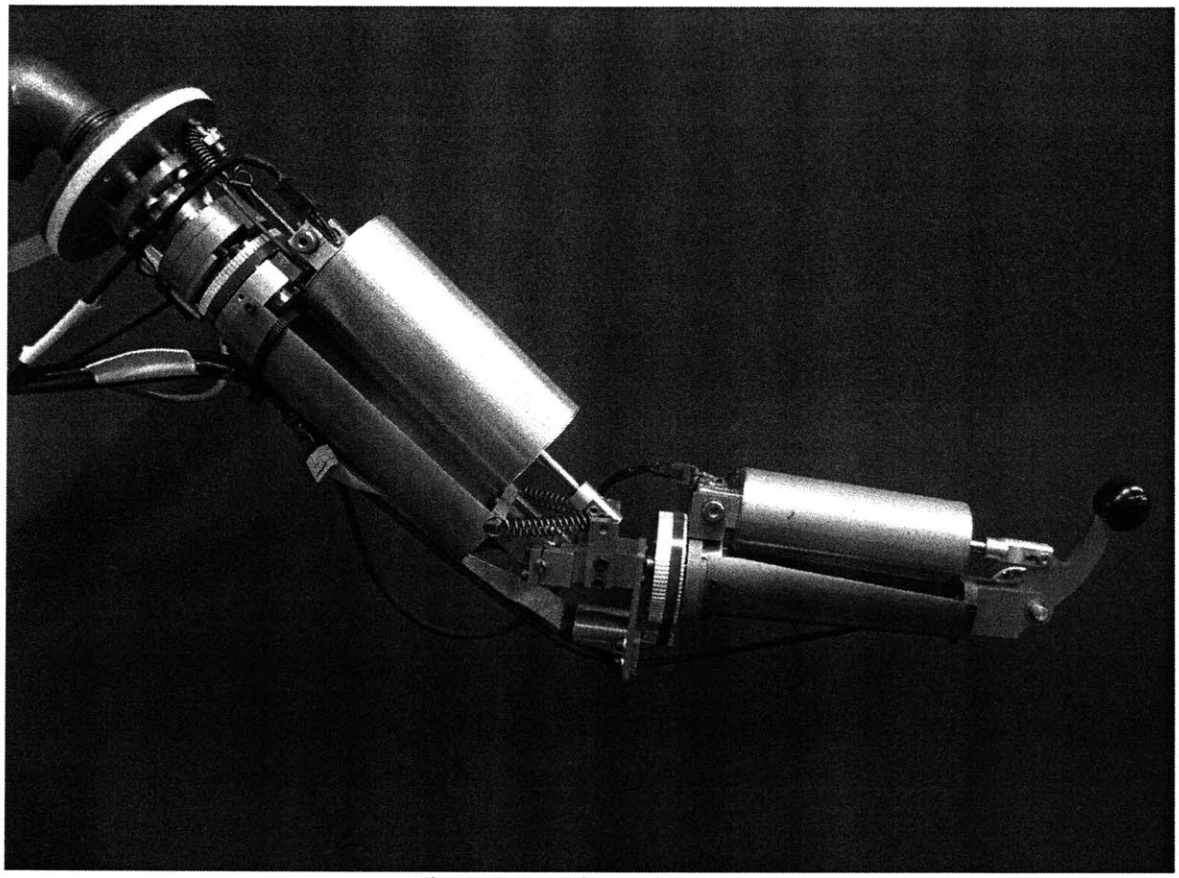

Figure 4.5 Photo of the arm

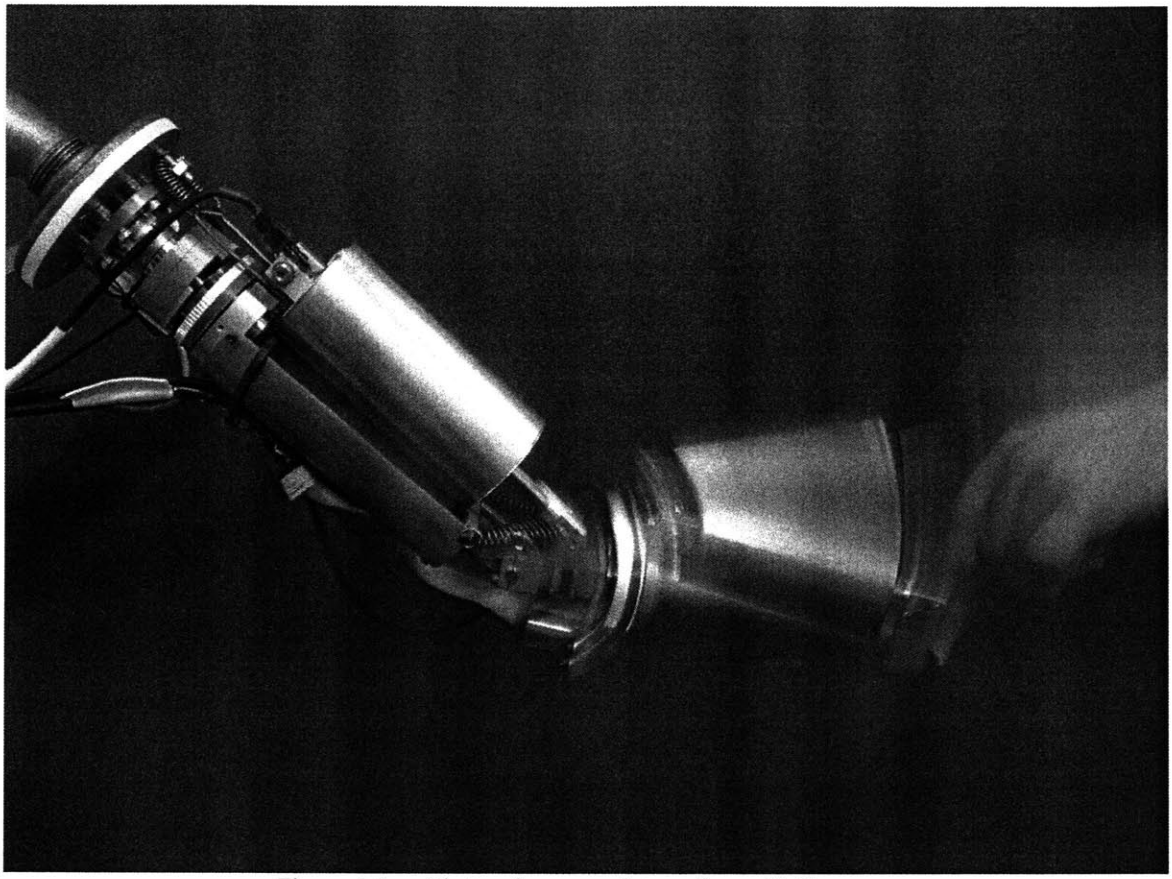

Figure 4.6 Photo of a person interacting with the arm

CHAPTER 5. KINEMATICS AND DYNAMICS

5.1 KINEMATICS

Figure 5.1 is a schematic of the 4 DOF arm. The 4 angles that describe the state of the arm are denoted by θ_b, θ_e, θ_f, and θ_w. θ_b and θ_f are the upper and lower roll angles, respectively. Their axes are aligned with the axes of their respective arm segments. Angles θ_e and θ_w are the angles of the VCA-actuated degrees of freedom, the elbow and the wrist.

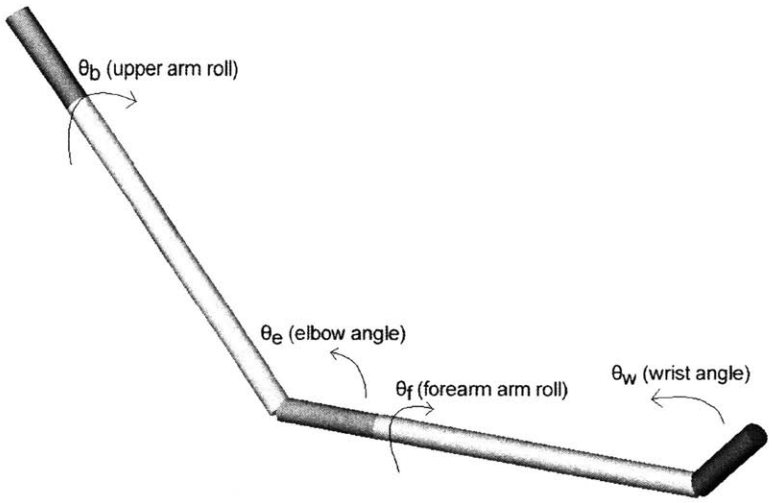

Figure 5.1 Schematic of kinematic arm structure

In the interest of conserving control bandwidth, all trajectory control tests were executed in joint space, eliminating the need for real time computation of large jacobian matrices. Conventional techniques for computing the inverse kinematics of a 4 DOF arm exist, but were not necessary to effectively evaluate the performance of the VCAs, the arm, and the controls systems developed.

With regard to the implementation of workspace-coordinate control systems (based on the end effector positions, solved using forward and inverse kinematics), it is important to note that the 4DOF arm is underconstrained with respect to the position of the end effector alone, necessitating a sophisticated control algorithm that introduces constraints between the different degrees of freedom, or imposes constraints on the orientation (in addition to the position) of the end effector. For example, such a constraint may attempt to keep the bicep joint angle as close to zero as possible, since it is the most costly to move in terms of power consumption.

5.2 DYNAMICS

The goal of implementing a model-based controller is to use knowledge of the system parameters to give the controller feedforward information that will enable better tracking performance for pre-scripted trajectories. Contrary to a gain scheduled controller, a full dynamic model provides a priori estimates of control inputs that account for position-dependant system parameters, desired state variables (and their time derivatives), and prescribed trajectories (and their time derivatives). For the development of such a model-based controller, simple PID controllers were used on the 2 roll degrees of freedom and the elbow, maintaining constant (zero) angles at those joints. This effectively reduces the 4DOF arm to a 1DOF planar arm, for the purpose of focusing very closely on the model and performance evaluation of the VCAs themselves. A full dynamic model was created for the 1DOF arm. The dynamic model takes into account inertial forces, viscous damping, gravitational forces, actuator winding resistance and inductance, position-dependant actuator attachment radius, and a position dependant actuator constant, accounting for the non-linearities within the VCA. The dynamic model for the VCA driving a 1DOF arm is:

$$i_i = [1/(K_{mi}Ri)]*[I_i\ddot{\theta}_i + M_i g l_{ci} Cos\theta_{gi} + K_{bi}\dot{\theta}_i]; \quad (2)$$

Where K_{mi} is the position-dependant VCA actuator constant, R_i is the position-dependant actuator attachment radius, I_i is the arm moment of inertia, $\ddot{\theta}_i$ is the angular acceleration of the joint, M_i is the mass of the arm, l_{ci} is the distance to the centroid of the arm, θ_{gi} is the gravitational angle of the joint (measured from horizontal), K_{bi} is the viscous damping constant for the joint, $\dot{\theta}_i$ is the angular velocity of the joint, and i_i is the current input to the VCA, which obeys the following first-order dynamics:

$$V_i = L_i\dot{i}_i + R_{ei}i_i; \quad (3)$$

Where V_i is the control input (voltage) to the actuator, and L_i and R_{ei} are the coil inductance and resistance, respectively. The following sections explain each of the terms in the above dynamic equations.

5.2.1 ACTUATOR CONSTANTS

K_{mi} is the VCA motor constant. Its units are N/Amp. Since the permanent magnet rotor travels within the coils, the interaction between the induced and permanent magnetic fields varies in strength, creating a position-dependant actuator constant. Effectively, the actuator constant can be regarded as:

$$K_{mi} = l_{ci} * B_i, \tag{4}$$

From (1), where l_{ci} and B_i are coil length and position-dependent magnetic field, respectively. This non-linearity has been measured for each actuator, and the profile of the position-dependent actuator constant, which is characteristic of both the bicep and wrist actuators, is shown in figure (5.2).

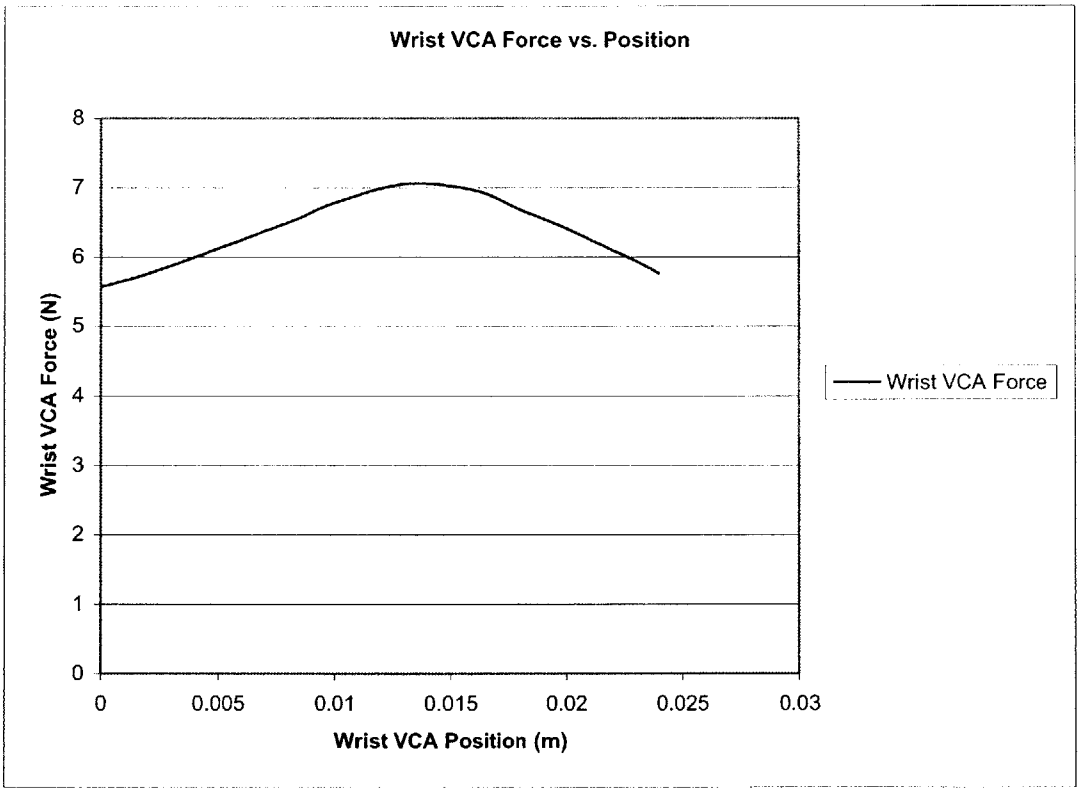

Figure 5.2 Plot of position dependancy of wrist actuator constant

For simplification, the relationship between actuator constant and joint angular position has been linearized as follows:

For $\theta_i \leq \theta_{imid}$:

$$K_{mi} = [(K_{i\max} - K_{i\min})/\theta_{imid}] * \theta_i + K_{i\min}; \quad (5)$$

For $\theta_i > \theta_{imid}$:

$$K_{mi} = [-(K_{i\max} - K_{i\min})/\theta_{imid}] * \theta_i + (K_{i\min} + 2(K_{i\max} - K_{i\min})); \quad (6)$$

Where K_{imax} and K_{imin} are the maximum and minimum actuator constants, $?_{imid}$ is the middle of the range of motion of joint i, and $?_i$ is the angle of joint i. For these calculations, K_{imax}, K_{imin} and $?_{imid}$ were measured empirically, for the best accuracy. This linearization describes an actuator profile as follows:

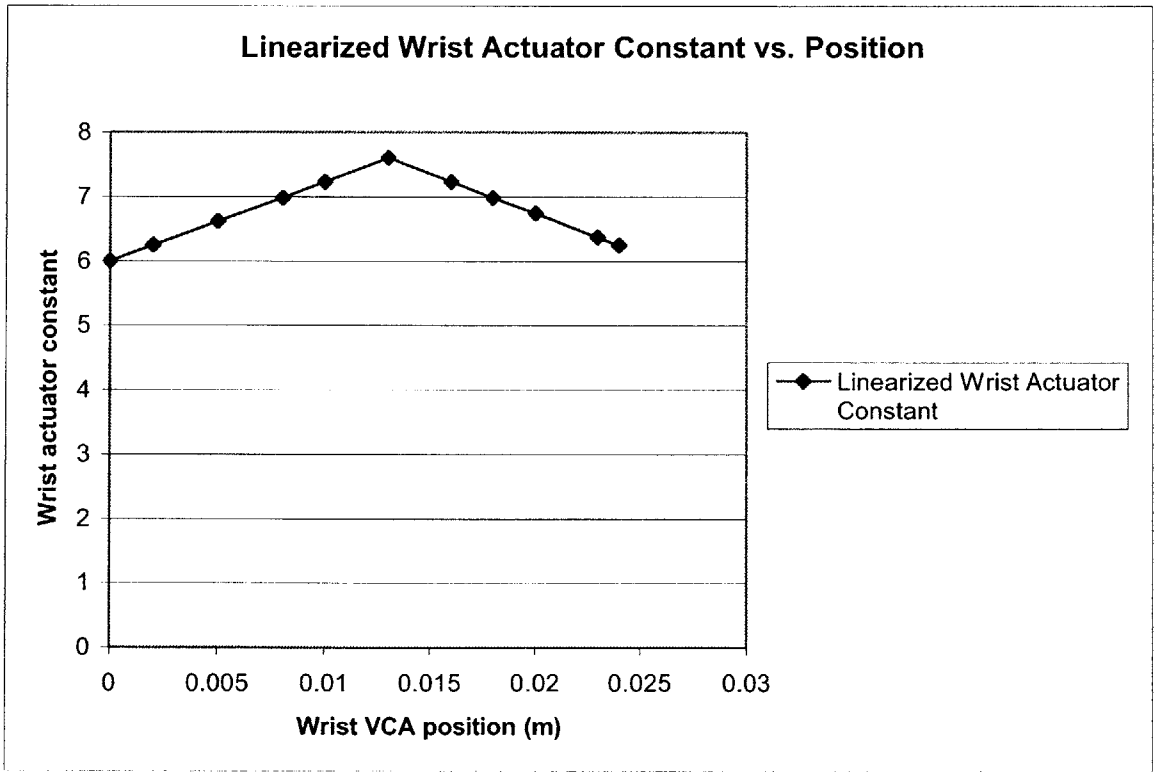

Figure 5.3 Linearization of position dependancy of wrist actuator constant

5.2.2 *Effective Actuator Attachment Radius*

R_i is the distance from the point of attachment of the actuator clevis to the axis of rotation of joint i, measured perpendicular to the axis of actuator i. It is the distance R_1 in figure 5.4.

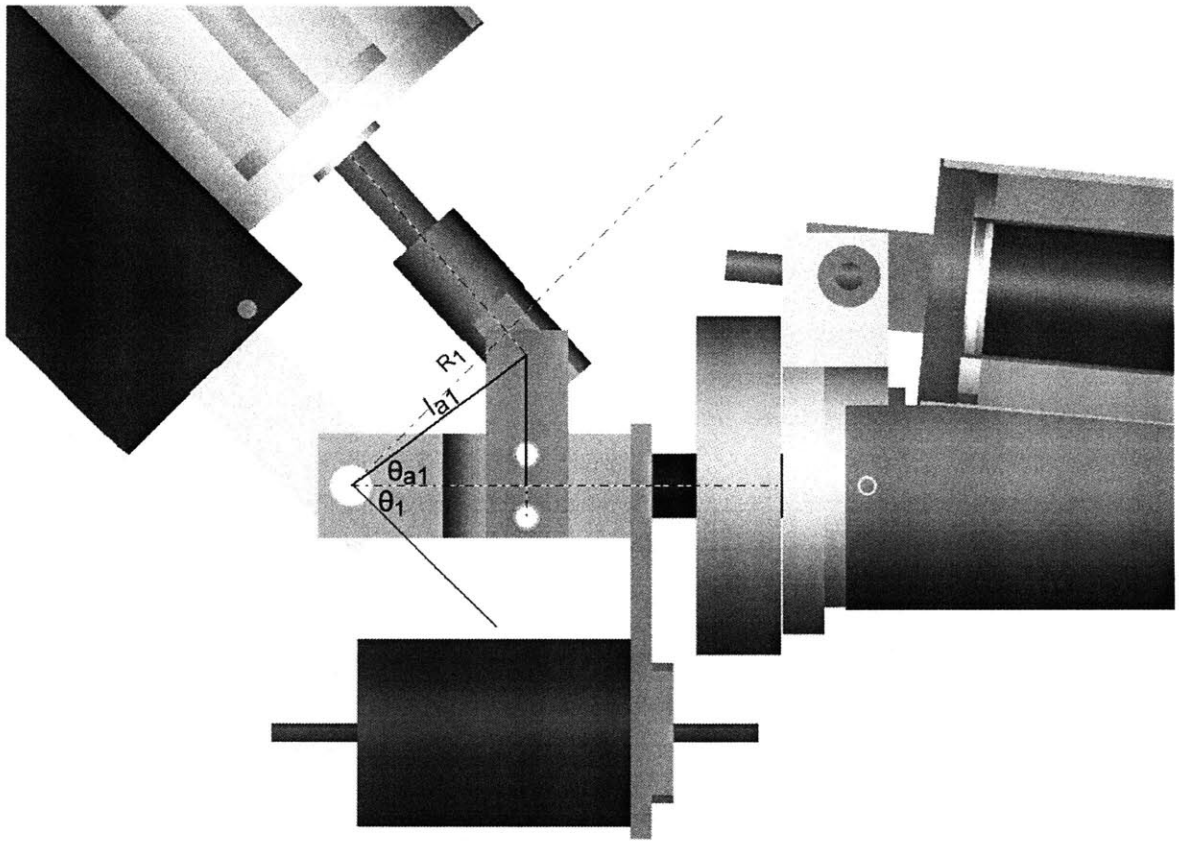

Figure 5.4 Schematic of position dependency of actuator attachment radius

R_i is clearly position-dependant, and it varies according to:

$$R_i = l_{ai} Cos(\frac{\pi}{2} - \theta_i - \theta_{ai}); \quad (7)$$

Where each of the parameters l_{ai}, θ_i, and θ_{ai} is defined in figure 5.4. For the calculation of R_i, the axis of the actuator is assumed to be parallel to the arm segment to which it is attached. In reality, this angle varies by less than 5°.

5.2.3 *Inertial and Gravitational Effects*

The first 2 terms in equation (2) represent the torques due to the inertia of the arm, and gravity. These are the dominant effects in the in the dynamic model for the arm. The gravitational term helps to minimize steady state position error, and the inertial term significantly improves tracking performance by adjusting the control signal based on desired acceleration in place of desired position alone.

5.2.4 *Viscous Damping*

The model includes a small amount of viscous damping. The primary source for velocity-dependant damping is eddy current damping within the actuators, although small amounts of viscous damping are present due to friction in the rotary encoders, and the viscosity of the oil used on the actuator shafts.

5.2.5 *Electrical Dynamic Model*

A simple first-order model was used to represent the actuator coil electrical dynamics. Equation (3) shows this model, where L_i and R_{ei} are the measured coil inductance and resistance of the respective actuators. Given the large size of the actuators, and the small size of the arm segment, the electrical time constant of the actuator coils is significant, necessitating these terms in the dynamic model.

The resultant system model is third order, with voltages to the actuators as the control inputs, and angular positions of the joints (and their first and second derivatives) as state variables.

CHAPTER 6. CONTROL SYSTEM DESIGN

6.1 Overview

Three control systems were implemented on the arm, in attempts to explore the potential of VCAs as robotic actuators, and to exploit their best characteristics. The first control system developed is a basic PID controller with full state feedback. The PID controller was implemented on all 4 degrees of freedom, and basic trajectory tracking tasks were executed in joint space. The second control system developed is a PID controller with gain scheduling that varies the control gains to account for some of the dominant non-linearities in the actuators themselves, as well as in the construction of the arm. The gain-scheduled PID controller was implemented on all 4 degrees of freedom, and once again trajectory tracking tasks were executed in joint space. Third, a more sophisticated model-based controller was implemented on an individual VCA-driven joint, with dynamic model-based feedforward compensation in addition to PD feedback. A full dynamic model was created for one of the VCAs (the wrist actuator), in an attempt to characterize it well enough to improve controller performance. As a means of exclusively testing the dynamic model of the VCA itself, the model-based controller was only implemented on one degree of freedom, however, it can be extended to multiple degrees of freedom using conventional techniques [6].

6.2 PID Control System

The first control system implemented on the arm was a simple PID controller, implemented on all 4 degrees of freedom. No system model was used, and all non-linearities were ignored. Feedback gains were determined empirically, since parameters that were difficult to characterize determine the stability of the system.
The block diagram of the PID control system for the 4DOF arm is shown in figure 6.1.

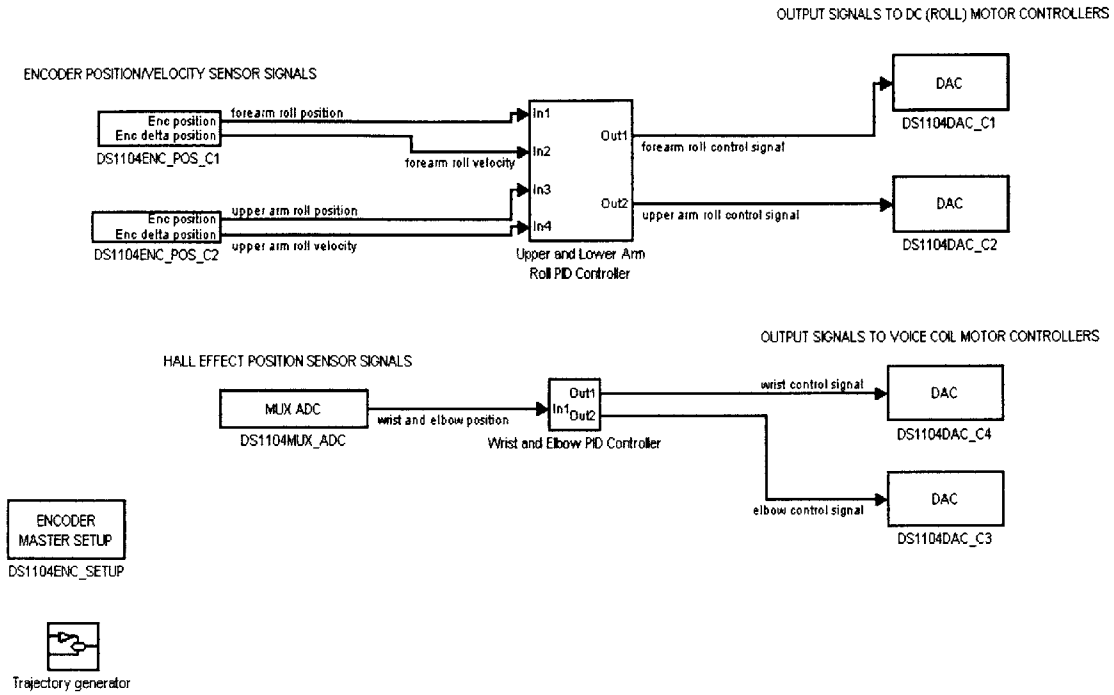

Figure 6.1 Block diagram of PID controller for 4DOF arm

Where the block diagram for the individual PID controllers is:

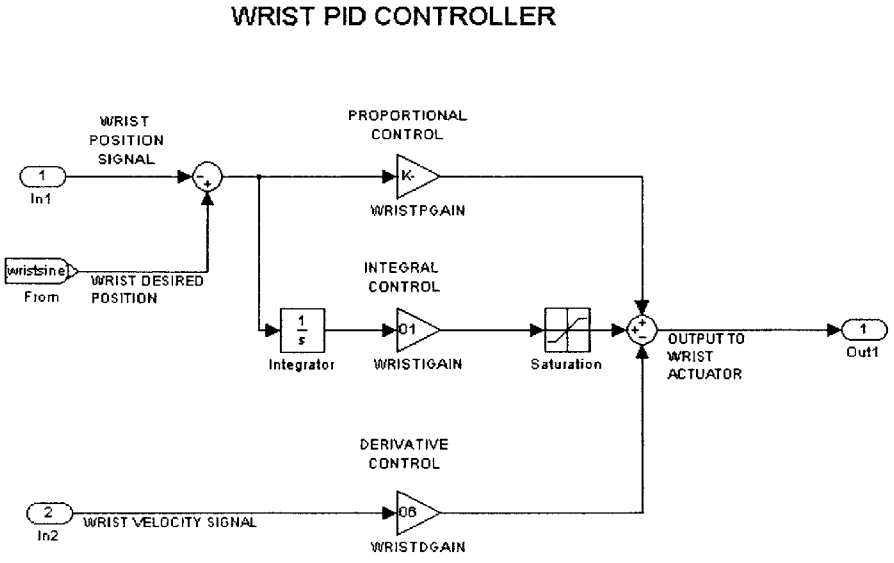

Figure 6.2 Block diagram of wrist PID controller

The PID control law is as follows:

$$V_i = -K_{pi}(\theta_i - \theta_{ides}) - K_{ii}\int(\theta_i - \theta_{ides}) - K_{di}\dot{\theta}_i \; ; \tag{8}$$

where V_i is the control input for joint i, $?_{ides}$ is the desired angular position of joint i, and K_{pi}, K_{ii}, and K_{di} are the proportional, integral and derivative control system gains, respectively.
Position and velocity information for the roll joints is obtained via magnetic encoders, and position information for the bicep and wrist joints is obtained via linear Hall-effect sensors. Consequently, the velocities of these joints are obtained by differentiating their position signals. As expected, high frequency electrical noise make this signal difficult to interpret, so low-pass filters with roll off frequencies of 100 rad/s were implemented on each of the position signals to be differentiated.

6.3 PID Control with Gain Scheduling

The next control system developed was a PID controller with a gain scheduling algorithm that varies the controller gains as functions of joint angular positions. Without developing a full system model, the gain scheduler adjusts the gains to compensate for the dominant non-linearities in the physical system. The system parameters for which gains were adapted were: position-dependant actuator constants, position-dependant actuator attachment radius, and position-dependant gravitational torques.

The block diagram of the PID Controller with gain scheduling is shown in figure 6.3.

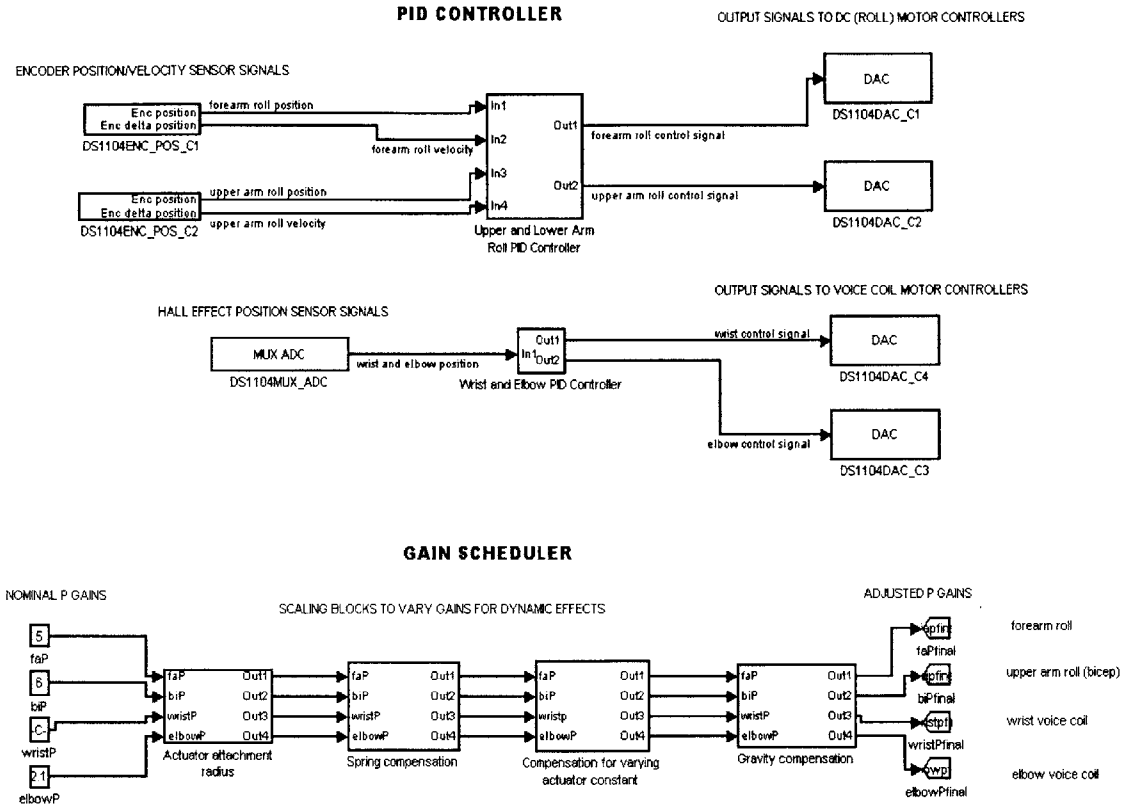

Figure 6.3 Block diagram of 4DOF PID control system with gain scheduling

The control law for the PID controller with gain scheduling is:

$$V_i = -K_{pi}(\theta_i - \theta_{ides}) - K_{ii}\int(\theta_i - \theta_{ides}) - K_{di}\dot{\theta}_i \; ; \tag{9}$$

the same as the PID control law, except that in this case the proportional control gains, K_{pi}, are position-dependant. The gains vary according to angular position of the joint, to compensate for non-linear gravitational effects, a varying actuator constant, and the non-linearity associated with the point of attachment of the VCA to the arm segment on which it acts. The dynamic models of these effects are discussed in section 5.2; the exact relationships between the proportional gains and the angular positions are described below, for each of the 3 effects.

6.3.2 *Position-Dependant Actuator Constants*

To counteract the position-dependant actuator constants of the VCAs, the controller proportional gains vary according to:

$$K_{pki} = K_{pinom} * (1 - \frac{K_{mi}}{K_{i\max}}) + K_{p\min}; \quad (10)$$

where K_{pki} is the proportional control gain adjustment factor, K_{pinom} is the nominal (starting) gain, to be adjusted by the gain scheduler, K_{pmin} is the minimum proportional control gain, and K_{mi} and K_{imax} are actuator constants, as defined by equations (5) and (6).

6.3.3 *Gravitational Effects*

Control gains were also adjusted to compensate for non-linear gravitational effects. The effect of gravity on the second joint (the wrist joint) is negligible, since the mass of this joint is very small. However, gravity plays a significant role on the torque seen at the bicep joint. Consequently, the following gain-scheduling law was implemented to vary the proportional control gain of the bicep VCA:

$$K_{pgi} = K_{pinom} * \frac{\tau_{gi}}{\tau_{gi\max}}; \quad (11)$$

where K_{pgi} is the proportional control gain adjustment factor, K_{pinom} is the nominal (starting) gain, to be adjusted by the gain scheduler, τ_{gi} is the varying gravitational torque (determined in equation (2)), and τ_{gimax} is the maximum gravitational torque experienced at the joint.

6.3.4 *Varying Radius At Which The VCA Acts on Arm Segment*

Thirdly, the effective radius at which the actuator clevis acts on its arm segment (and thus the torque delivered to that arm segment for a given force input) varies non-linearly with angular position of the joint. The proportional control gains were therefore varied for both the bicep and forearm VCAs according to the following gain-scheduling law:

$$K_{pri} = K_{pinom} * (1 - \frac{R_i}{R_{i\max}}) + K_{p\min}; \tag{12}$$

where K_{pri} is the proportional control gain adjustment factor, K_{pinom} is the nominal (starting) gain, to be adjusted by the gain scheduler, R_{i} is the varying actuator radius of attachment, R_{imax} is the maximum actuator radius of attachment, and K_{pmin} is the minimum proportional control gain.

Ultimately, the control system proportional gain is adjusted according to:

$$K_{pi} = K_{pki} * K_{pgi} * K_{pri} \tag{13}$$

6.4 *Model-Based Control System with PD Feedback*

Finally, a controller for the wrist VCA was designed with a feedforward term based on the dynamic model discussed in section 5.2, in addition to a simple PD feedback term. The block diagram of the Model-based control system with PD Feedback is shown in figure 6.4.

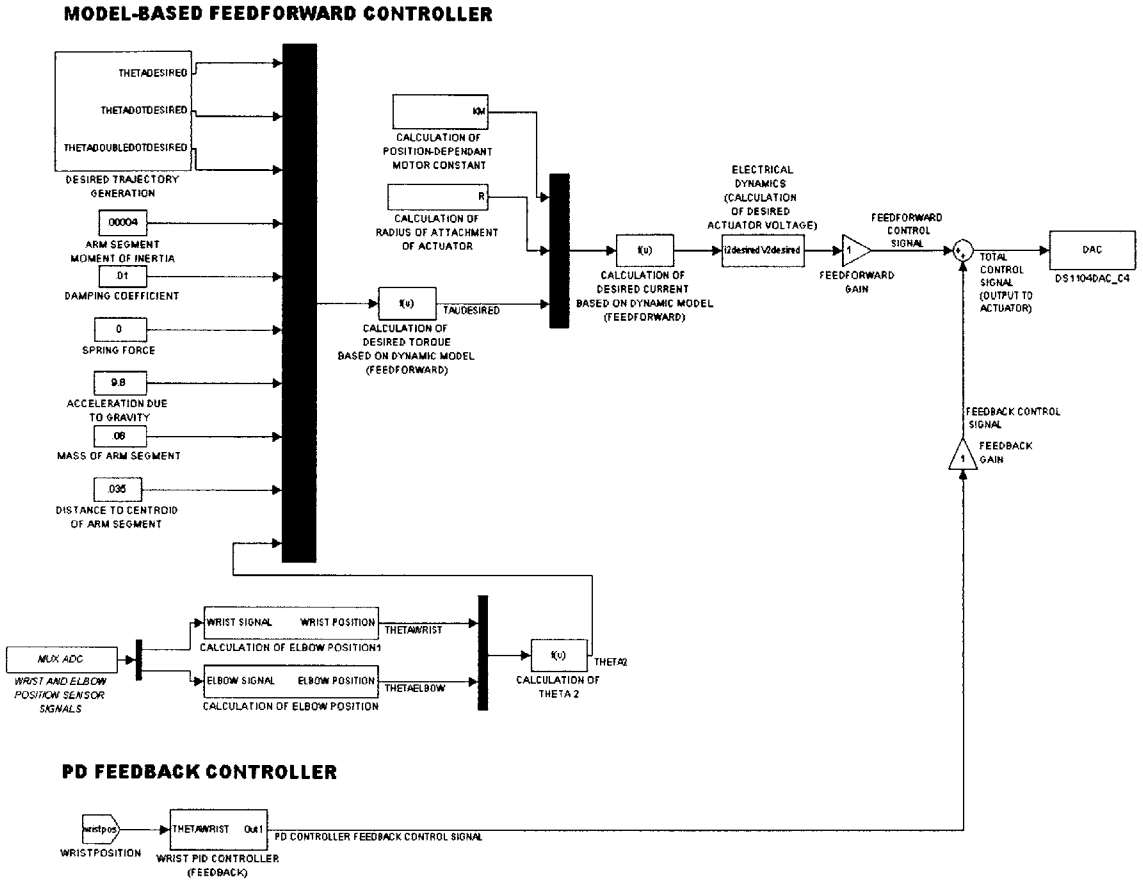

Figure 6.4 Block diagram of model-based controller with PD feedback

The model-based control law is:

$$V_w = \hat{V}_w - K_{pw}(\theta_w - \theta_{wdes}) - K_{dw}\dot{\theta}_w; \tag{14}$$

Where $\hat{V}_w$ is the calculated desired input voltage to the wrist actuator, from (2), (3), (5), (6), and (7), based on desired angular position, velocity, and acceleration, and based on estimates (and measured values) of each of the constant parameters in the dynamic model. The second and third terms in the control law represent the PD (feedback) portion of the controller. The controller uses the feedforward term, $\hat{V}_i$, to provide best-estimate control signals to track a prescribed trajectory in an open-loop fashion, and corrects for imperfections in the model (via the proportional control term) by observing and comparing actual joint positions (using feedback sensors) with desired positions, and adjusting the control input accordingly. The third and final term in the control law provides some damping to the system to minimize overshoot and smooth the motion of the arm.

Table 6.1 shows each of the relevant estimated and measured parameters in the dynamic model. Some of the constant parameters (l_{c2}, for example) do not appear explicitly in the dynamic equations, but are used in the derivations of some of the terms.

Table 6.1 ARM AND ACTUATOR DESIGN PARAMETERS RELEVANT TO WRIST CONTROL SYSTEM DEVELOPMENT

Parameter Name	**Description**	**Estimated or Measured Value**
L_2	Inductance of wrist actuator	3.2 mH
Re_2	Electrical resistance of wrist actuator	3.715O
K_{2max}	Peak wrist actuator constant	7.6 N/A
K_{2min}	Minimum wrist actuator constant	6.2 N/A
θ_{2mid}	Half-stroke wrist angle	0.855 rads (49°)
l_{a2}	See figure 5.4	0.0224 m
θ_{a2}	See figure 5.4	0.262 rads (15°)
m_2	Mass of hand	0.08 kg
I_2	Moment of inertia of hand	$3.75x10^{-5}$
l_{c2}	Distance from wrist axis to centroid of hand	0.03 m
g	Acceleration due to gravity	9.8 m/s^2

CHAPTER 7. RESULTS

7.1 ACTUATOR RESULTS

Despite not being optimized for cost, force, or power density, the VCAs developed show promising results as robotic actuators. Their simple design affords cheap, fast construction. Their concentric form factor enabled smooth integration into the robot arm, and minimized the number and size of bearings that were necessary. A light lubricant was used on the actuator shafts, resulting in extremely low mechanical Coulombic and viscous friction, and completely silent actuation. The actuators have high bandwidths and are easy to control. They are backlash and cog-free, and their low friction characteristics permit high control system gains. They have some inherent damping due to back EMF, which, when used in conjunction with a damping term in the control law, allows fluid, smooth, life-like motion.

7.1.1 PERFORMANCE

The VCAs performed according to specifications they were designed to meet. The maximum 10-second peak pressure was approximately 50KPa, which is approximately $1/7^{th}$ that of human muscle. Significantly higher pressures are achievable for shorter durations. Peak actuator constants are 16.2 N/Amp and 7.1 N/Amp for the bicep and wrist actuators, respectively. The force performance curves are shown in figure 7.1.

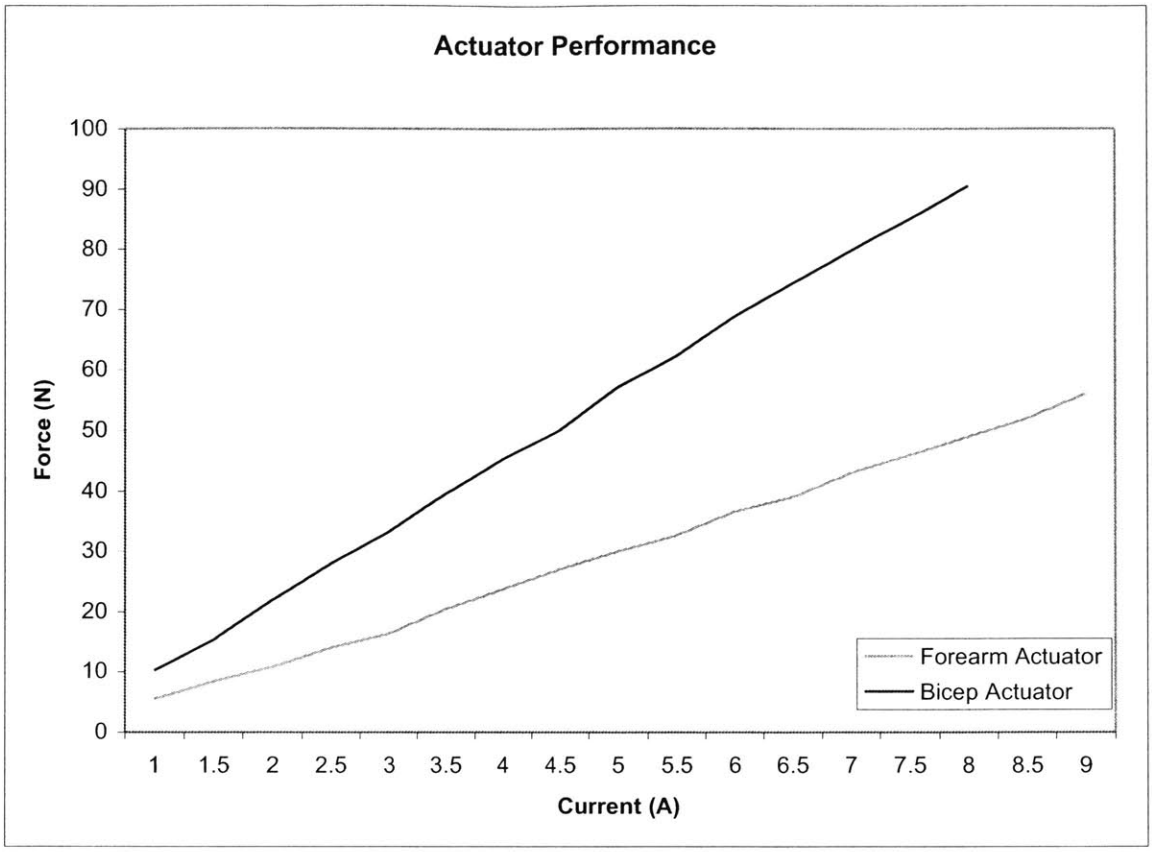

Figure 7.1 Plot of forearm and bicep actuator force performance

As the figure shows, the actuator performance is roughly linear over a broad range of currents (and temperatures) – a linearity that could be exploited to obtain information regarding arm loading, or to use current measurements to implement basic force control without the use of expensive and cumbersome force sensors. In an attempt to compare VCAs with some of the other forms of actuation discussed in table 2.1, table 7.1 shows some of the measured results of key actuator performance metrics for the VCAs. Some metrics are only discussed qualitatively (noise level, for example), as absolute measurements may be difficult to obtain or characterize.

Table 7.1 ACTUATOR PERFORMANCE RESULTS

Performance Metric	Value	Discussion
Peak Pressure	50 kPa	This value is conservative. Destructive tests were not conducted. This is approximately 4-7 times lower than human muscle.
Peak Volumetric Power Density	1.26 MW/m^2	Efficiency is speed dependant – this value assumes a total efficiency of 50%
Peak Mass Power Density	300W/kg	Approximately 50% higher than human muscle
Peak Volumetric Force Density	470kN/m^3	Relatively low – characteristic of electromagnetic actuators
Peak Mass Force Density	112N/kg	Relatively low due to the high density of magnetic materials used. A problem that future research should address
Maximum Strain	38%	Strains up to 50% are easily obtained, at the cost of inefficiency due to heating in the coils
Work Density	5.6J/kg	High material density hurts this value, but long achievable strains help offset the effects of the high actuator mass
Speed	Fast	A conclusive test was not conducted, but smooth actuator response is achievable well above 100 Hz.
Noise level	Silent	Silent at any speed – a strong advantage of voice coils
Bicep actuator mass	1.37kg	
Wrist actuator mass	0.5kg	

7.1.2 *Shortcomings*

As can be seen in chapter 6, a major shortcoming of the VCAs from the control standpoint is their inherent non-linearity. Several properties of VCAs make them prone to non-linear torque delivery, when used as robotic actuators. Many of these properties have been exposed in this thesis, including position-dependant actuator constants, and the sinusoidally-varying torque delivery that results from using a linear actuator to drive a rotary joint. These non-linearities, however, can be modeled without much difficulty, and control strategies can be very effective at overcoming them. Also, careful geometric decisions can counteract some of the resultant deficiencies. For example, as the actuator constant weakens significantly near the end of the range of motion of the VCA, springs can be used with force characteristics that oppose this effect.

Clearly, the mass of the actuators is a concern, and an area for future development as well. Research has been done in the areas of fluid cooling for electromagnetic actuators, lightweight, high permeability magnetic materials, and increased air gap flux density. Research such as this will push VCAs toward being lighter and stronger, and therefore more competitive as robotic actuators.

7.2 *Arm Results*

The arm is both an effective evaluation platform for the VCAs, as well as a promising prototype of a dextrous, interactive arm for future robots in the Robotic Life Group. The arm moves smoothly, quickly and quietly enough to communicate effectively and convincingly. It has ample strength to perform useful tasks, such as holding a tool or a part, opening a door, or lifting a light object. In addition, the arm has the strength, agility, and quality of motion to execute complex tasks such as surface tracing or catching and throwing, if an appropriately sophisticated control system is used.

7.2.1 *Interactivity*

Interactions with the arm are compliant and safe. The inherent backdriveability of the actuators gives the arm an organic feel, despite its strength. As a result of the arm's compliance, collisions with objects or people in its environment are not damaging to the arm, its actuators, or the objects or people with which it is colliding. The silence and speed of the actuators further enrich the interaction, making it more human-like.

7.2.2 *Strength*

The Voice coil actuators have peak forces approximately 11 times greater than their weights, making them very suitable for this robotic application. The design goals discussed in table 3.1 were met, and end effector forces of 20 N were realized. This is adequate strength for a robot of this size to effectively execute low-moderate force tasks (shaking hands, pushing objects, holding and using various tools – screwdrivers, a drill,

or a hammer, for example). This strength also allows accelerations that permit the robot to exhibit a range of emotions (shock, surprise, and excitement, for example) in convincing and organic ways.

7.3 Overall System Results (with controllers)

The implementation of different control systems on the arm and actuators further highlighted the strengths and weaknesses of VCAs as robotic actuators, as well evaluating the utility of this type of robotic arm in a robot intended for human interaction. Since the actuators and the mechanical system were designed with fluid, silent, high-bandwidth, backlash-free motion in mind, it is important that no other components in the system compromise this performance. For relatively low control system gains, the motor controllers behaved predictably and smoothly. The result is reasonable tracking performance at low frequencies, using all types of control systems that were tested. At higher frequencies, the simpler control systems (such as the basic PID controller) preserved the smoothness of motion, despite poor trajectory tracking performance. The model-based controller, however, exhibited excellent quality of motion and trajectory tracking performance and a wide range of frequencies.

Control system gains were kept low for the evaluation of the arm for several reasons. First, low-stiffness, heavily damped motion was desired to ensure safe interaction, and smooth arm motion. Consequently, fast, stiff actuator responses were sacrificed for an organic quality of motion. Secondly, the upper and lower arm roll degrees of freedom are clearly the weak link in the arm design, meaning that at high gains (or high accelerations) these actuators saturate. Keeping gains low permitted smoother, more linear responses from these actuators. Thirdly, jitter problems in the digital amplifier restricted the permissible control system gains. Beyond a certain gain threshold, the response of the elbow actuator to externally applied loads was an erratic, high frequency tremble. The high bandwidth of the VCAs make them sensitive to such jitter in the control signal, despite filtering. Finally, characteristics of the components used in the arm design imposed limits on permissible controller gains. Differentiated noisy signals from the Hall-effect sensors at the elbow and wrist joints forced low damping gains for these joints, and a structural resonance of the arm at approximately 36 rads/sec made high frequency, high stiffness trajectory control difficult. Such a structural problem could be solved in the future by implementing compliance and dampening elements at the shoulder.

7.3.1 Results with PID controller

The trajectory tracking performance using the simple PID controller is shown in figures 7.2 thru 7.5. The desired trajectories for each of the 4 degrees of freedom are simultaneous sinusoids with frequencies of 9rads/s. Understandably, the 2 degrees of freedom with the highest inertial loads have the worst tracking performance. The

tracking performance is reasonable at this, and lower frequencies, with maximum phase lags of approximately 0.88 radians for the elbow and upper arm roll degrees of freedom.

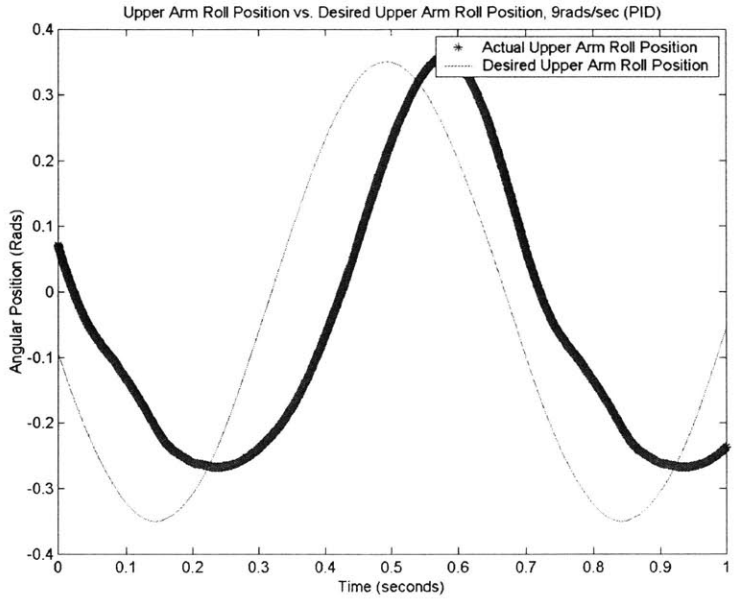

Figure 7.2 Upper arm roll tracking performance with PID control (9 rads/sec)

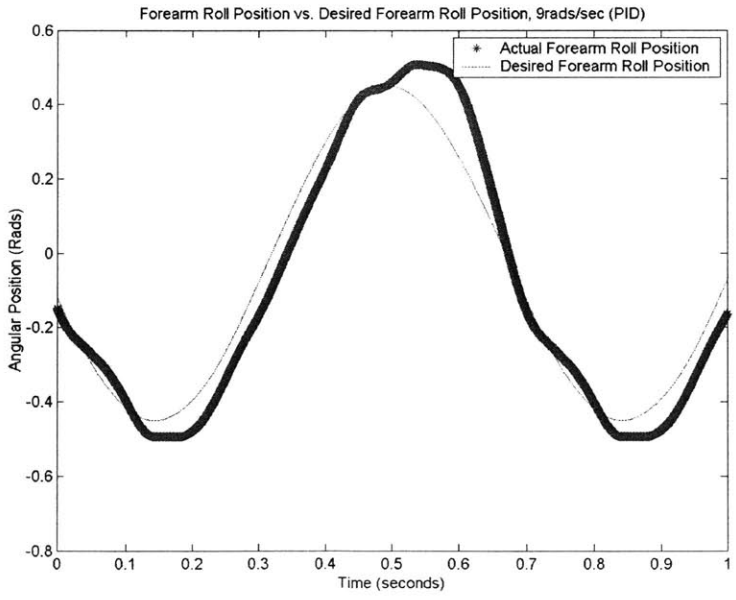

Figure 7.3 Forearm roll tracking performance with PID control (9 rads/sec)

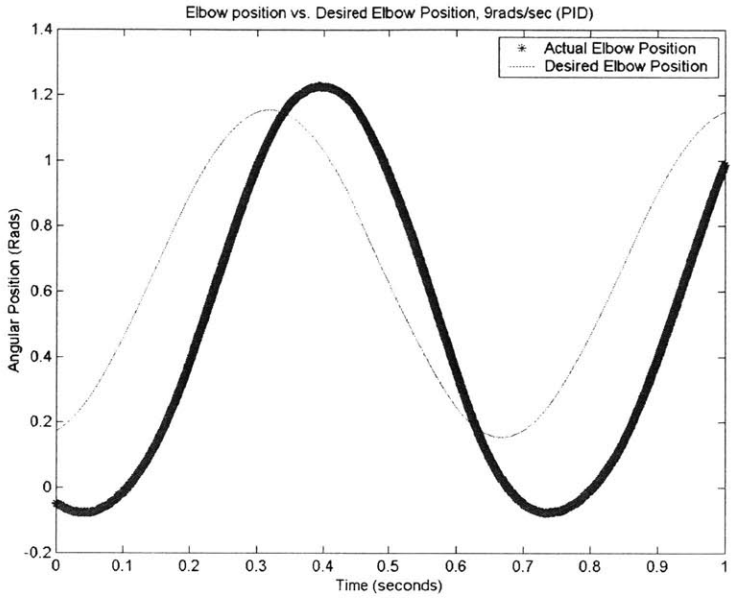

Figure 7.4 Plot of elbow tracking performance with PID control (9 rads/sec)

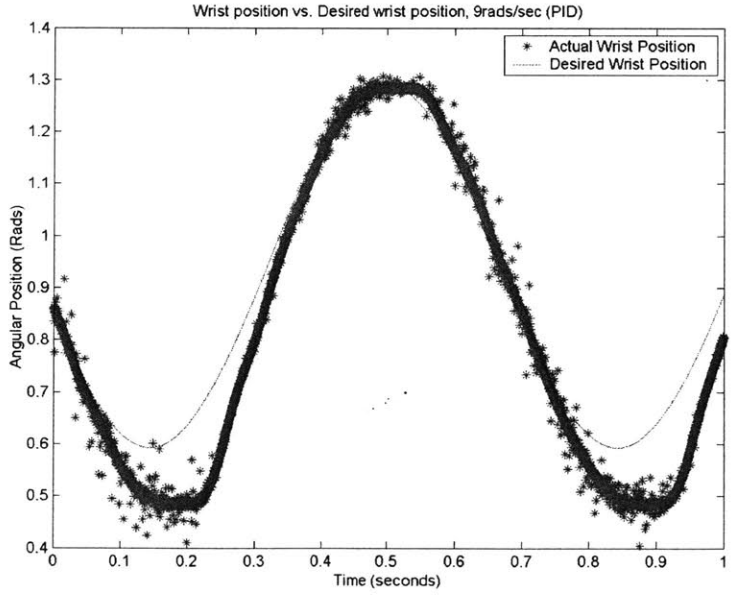

Figure 7.5 Plot of wrist tracking performance with PID control (9 rads/sec)

7.3.2 *Results with PID controller with Gain Scheduling*

The same trajectory tracking task was executed with the PID controller with gain scheduling. While some marginal improvements were noticed over the PID controller, the trajectory tracking performance was largely the same as that of the PID controller. The most significant improvement is the decreased overshoot of the elbow actuator, as a result of the modeling of the gravity-compensating springs at the elbow joint. The lack of improvement of the gain scheduling controller over the PID controller implies that the dominant effects affecting the controller performance are not the effects for which the control gains were adjusted. Specifically, the inertial and damping effects play a major role in the arm's response, as can be seen by the performance of the model-based controller. The gain scheduler is affected very little by external forces acting on the arm. The gains are bounded such that they remain within a stable range, regardless of the state of the arm, or of the external load. The trajectory tracking results for the PID controller with gain scheduling are shown in figures 7.6 thru 7.9.

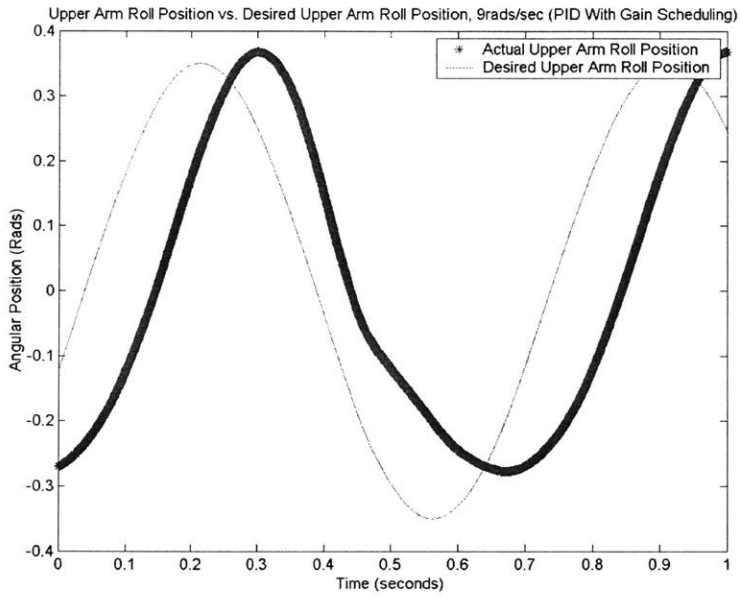

Figure 7.6 Plot of upper arm roll tracking performance with PID controller with gain scheduling (9 rads/sec)

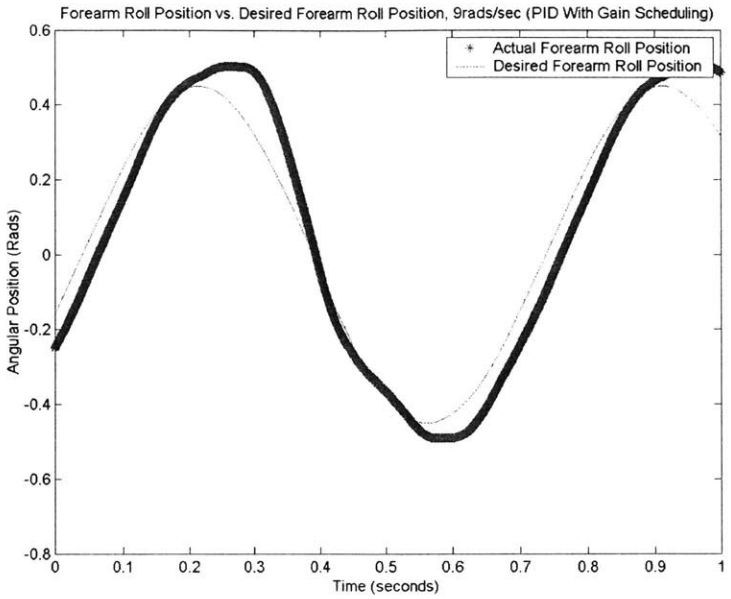

Figure 7.7 Plot of forearm roll tracking performance with PID controller with gain scheduling (9 rads/sec)

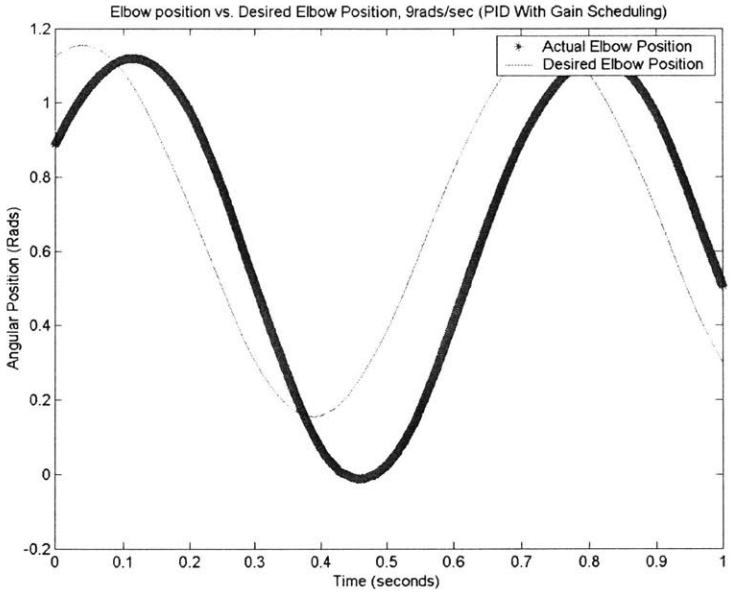

Figure 7.8 Plot of elbow tracking performance with PID controller with gain scheduling (9 rads/sec)

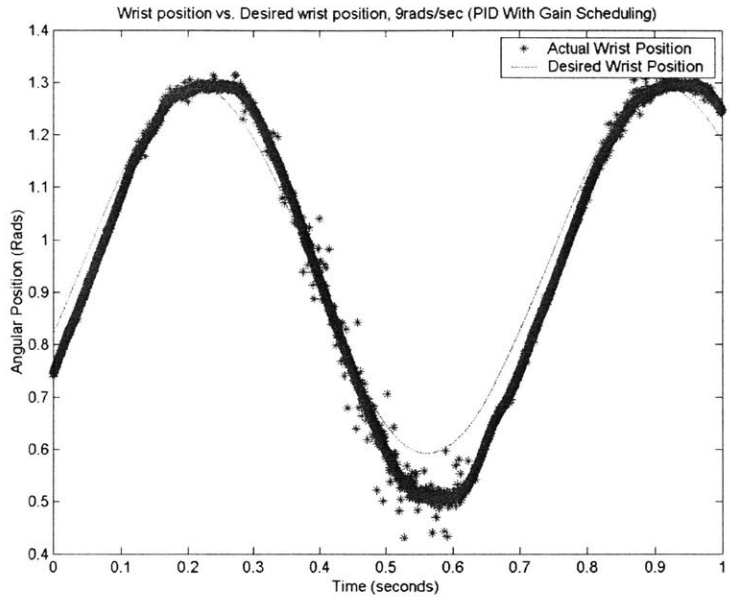

Figure 7.9 Plot of wrist tracking performance with PID controller with gain scheduling (9 rads/sec)

7.3.3 Results with Model-Based Feedforward controller with PD feedback

The arm exhibited excellent tracking performance with the model-based controller. A sinusoidal trajectory tracking task with a frequency of 40rads/sec was implemented first with the feedback controller alone, then with the feedforward term added. The results of these two tests are shown in figures 7.10 and 7.11. Under feedback control only, the response is diminished by almost 50%, and the joint position lags the desired position by 90°. With the feedforward controller, the tracking performance is extremely tight. The joint position lags the desired position by less than 10°, and the amplitude of the position is within 1% of the desired amplitude. Clearly the dynamic model (especially the representation of the arm's inertia) offers a great advantage over the simpler control systems.

Despite the arm's excellent trajectory tracking performance with the model-based controller, this controller is limited in its relevance for tactile interaction with the arm. Unless the external force (in our case, most often a human) is included in the system model, the controller can do nothing other than rely on the feedback portion of the controller to maintain appropriate pressure. Once contact is established, the model has little effect in helping the system respond to the external disturbance. The lack of feedforward compensation, however, did not cause stability problems, as the feedback gains remain constant, and the feedforward control inputs are bounded due to the inertia, mass, and desired trajectories being bounded.

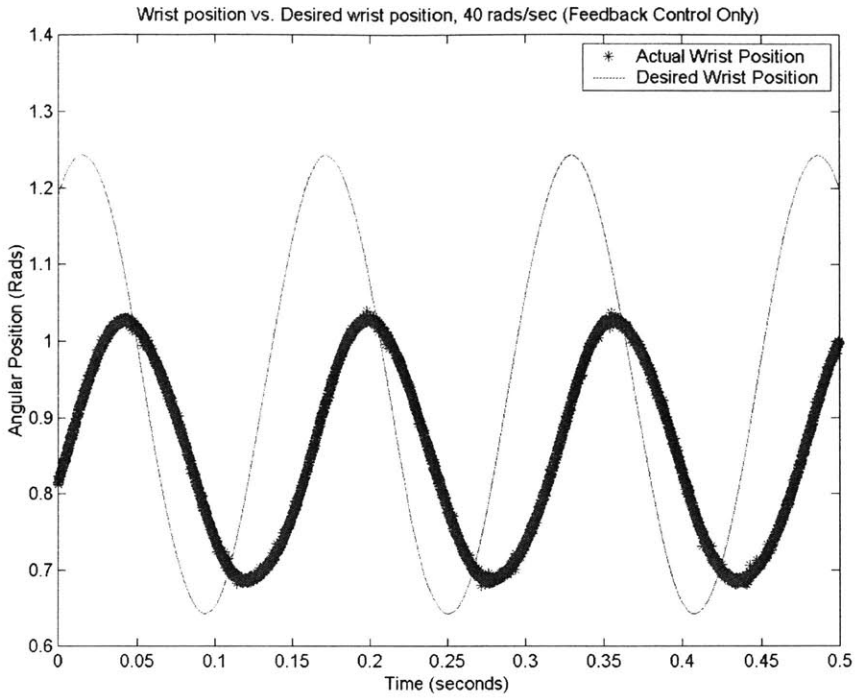

Figure 7.10 Wrist actuator tracking performance with PD control, 40 rads/sec

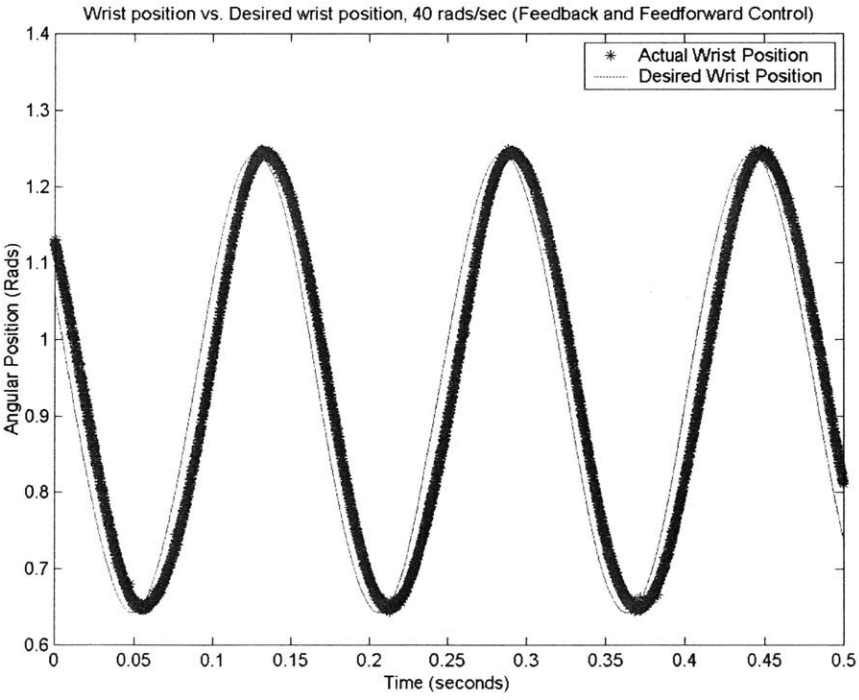

Figure 7.11 Plot of wrist actuator tracking performance with feedforward and feedback control, 40 rads/sec

Secondly, the step response performance of the model-based controller was compared to that of the simple feedback controller. It can be seen from figures 7.12 and 7.13 that, while the step responses of the two controllers are similar (due to very low control gains), the steady state position error is significantly reduced by the model-based controller, due to the gravity compensation in the dynamic model.

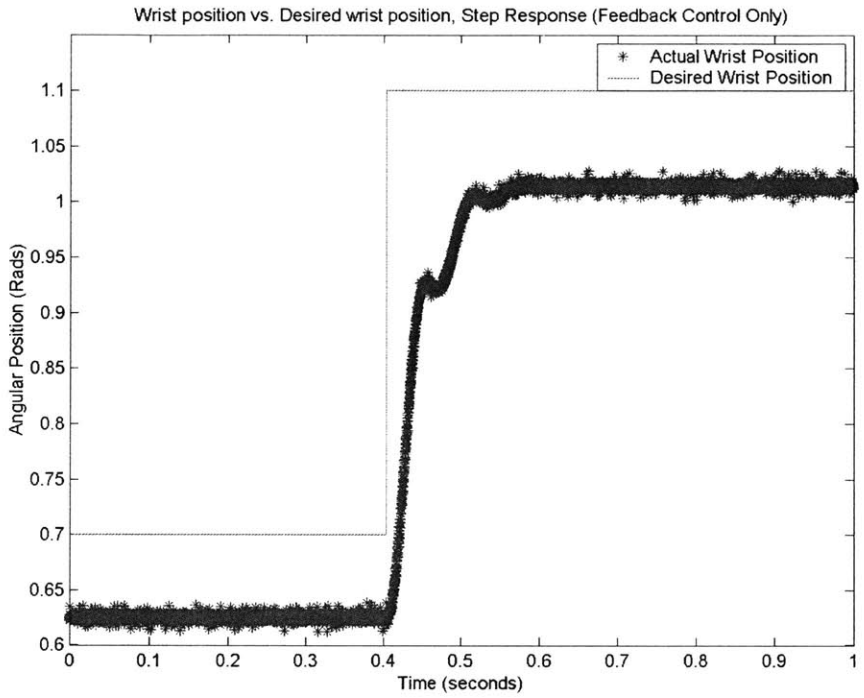

Figure 7.12 Plot of wrist actuator step response with simple PD control

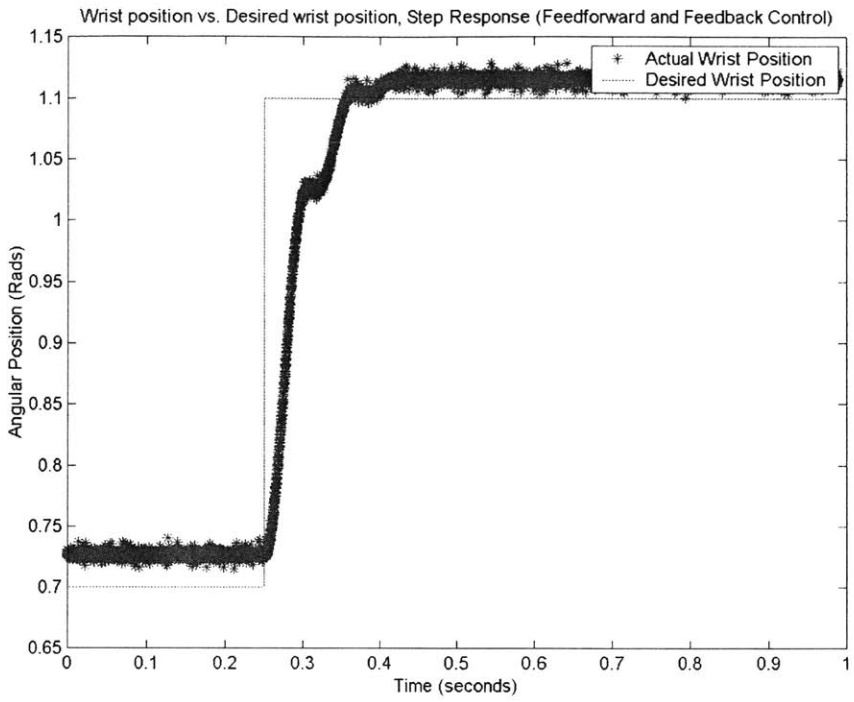

Figure 7.13 Plot of wrist step response with feedback and feedforward control

Finally, a test was performed to determine at what frequency the model-based controller became ineffective. Figure 7.14 shows the results of an 80rads/sec sinusoidal tracking task, in which the performance of the model-based controller is greatly diminished. The model-based controller gave tracking performance within 20° of phase lag and 10% amplitude matching at frequencies up to 55 rads/sec.

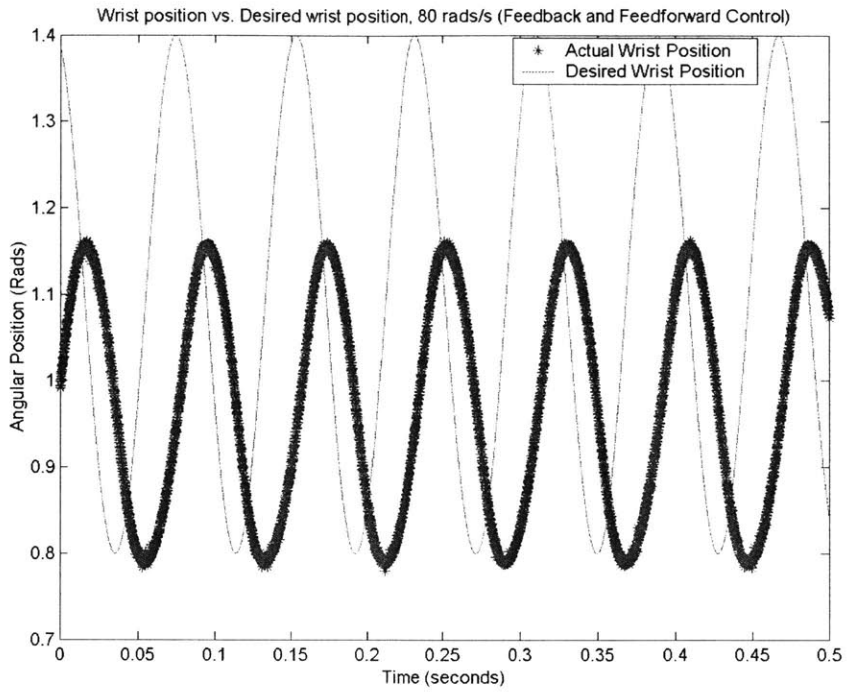

Figure 7.14 Plot of wrist actuator tracking performance with feedforward and feedback control, 80 rads/sec

CHAPTER 8. FUTURE WORK AND CONCLUSION

8.1 Future Work

This research has demonstrated the viability of VCAs as robotic actuators, and has highlighted their major deficiencies. These deficiencies include: high actuator mass, low actuator pressure, non-linearities that complicate control, and inefficiency at low speeds. Two major veins of future work would greatly benefit the development of VCAs as robotic actuators.

First, research into the design and materials used in VCAs would help resolve some of the fundamental problems with VCAs mentioned above. Novel, low-impedance mechanical transducers could be developed to address the problem of low actuator pressures. Further to that cause, research in the area of low resistivity coil materials or improved heat dissipation would help to increase actuator pressures by allowing more current to flow in the coils, potentially without a decrease in efficiency. Most importantly, materials with higher magnetic remanences, higher heat tolerances, and lower densities would greatly reduce the mass of VCAs, while increasing actuator performance.

Secondly, development of sophisticated control systems designed specifically for VCAs will enrich the interaction between humans and robots, and enable more useful tasks to be accomplished. Such tasks (grasping an object or shaking hands with a person, for example) depend heavily on control system design. For convincing tactile interactions, force, impedance, or hybrid control [16] will be necessary to fully take advantage of the VCAs' excellent quality of motion. In the near future, a 4DOF force-sensing hand will be mounted on the arm for experimentation with end-effector force control.

In an attempt to tackle the low pressure problem associated with VCAs, we have conducted preliminary research on compact electro-hydraulic systems that marry the high power densities of electromagnetic actuators with the high pressures of hydraulic actuators. We believe that a strong potential exists in using a voice coil-driven miniature hydraulic pump, packaged within a hydraulic actuator (cylinder) to leverage some of the benefits of the two forms of actuation. Such an actuator could eliminate the need for hydraulic lines and valves, while taking advantage of the strong, fluid motion of hydraulic systems, the form factor of the two forms of actuation, their quiet and controllable operation, and their high power densities. Fig. 8.1 shows our prototype of a self-contained electro-hydraulic actuator comprising a brushless DC motor, a miniature gear pump, and bellows-style pistons at either end. The system is fully sealed, and the motor operates submerged in the working fluid. Initial results have revealed that VCA-piston pump designs may afford higher pressures and efficiencies.

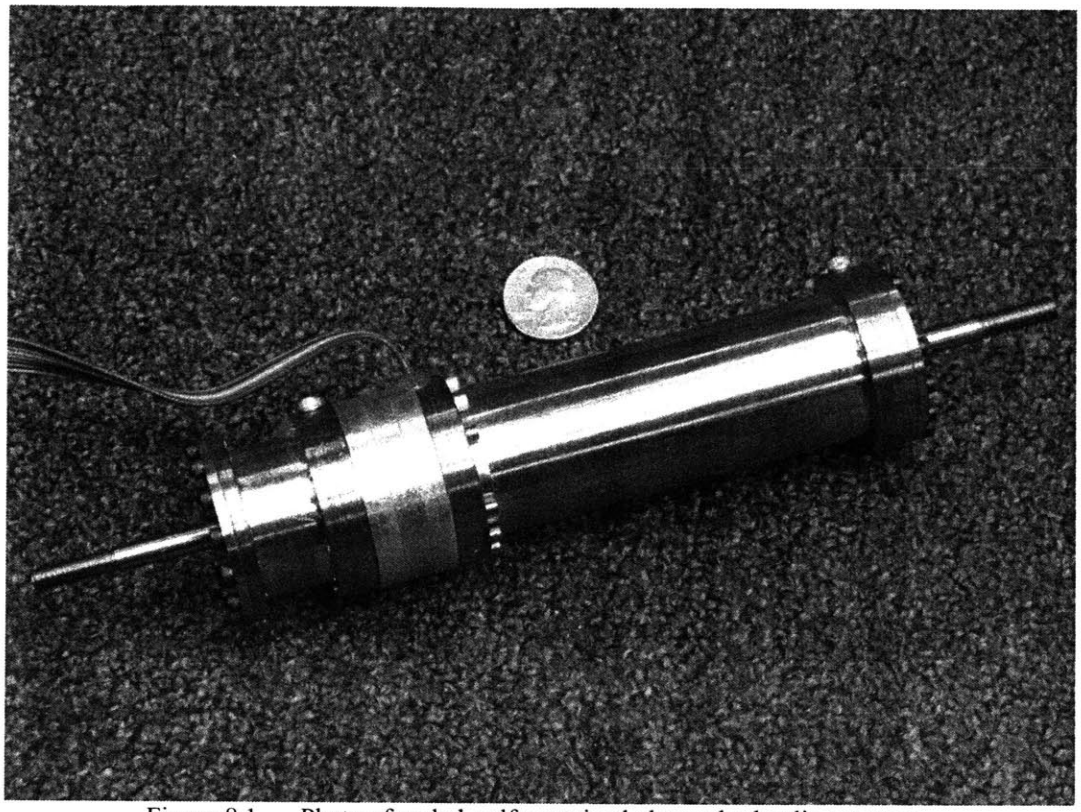

Figure 8.1 Photo of sealed, self-contained electro-hydraulic actuator

8.2 Conclusion

The advantages and compromises in using VCAs as actuators for HRI robots is evident. They have been chosen for their high quality of motion, fast response, controllability, and form factor. The tradeoff is that they are less efficient at low speeds than other actuation technologies, and must be oversized due to their low pressures. This preliminary study has shown that, for applications to medium DOF, non-mobile robots for tactile interaction with people, this tradeoff is acceptable.

BIBLIOGRAPHY

[1] J. Hollerbach, I. Hunter & J. Ballantyne "A comparative analysis of actuator technologies for robotics", O. Khatib, J. Craig & Lozano-Perez Eds, *The Robotics Review* 2, MIT Press, Cambridge MA 1992, pp. 299-342.

[2] J. Madden, N. Vandesteeg, P. Anquetil, P. Madden, A. Takshi, R. Pytel, S. Lafontaine, P. Wieringa, and I. Hunter, "Artificial Muscle Technology: Physical Principles and Naval Prospects", under review, submitted to *The Journal of Oceanic Engineering, 2004.*

[3] Y.Bar-Cohen, Ed, "Electroactive Polymer (EAP) Actuators as Artificial Muscles, Reality, Potential, and Challenges", SPIE Press, 2001.

[4] S.E. Salcudean and L. Stocco, "Isotropy and Actuator Optimization in Haptic Interface Design", IEEE International Conference on Robotics & Automation (San Fransisco, CA) April, 2000.

[5] Anthony C. Morcos, "Voice Coil Actuators for use in Motion Control Systems", online content available at: http://www.motion.org/9804morc.htm, 1998.

[6] H. Asada and J-J. Slotine, "Robot Analysis and Control", Wiley Interscience, 1986.

[7] Y. Bar-Cohen, Online content available at: http://ndeaa.jpl.nasa.gov/nasa-nde/lommas/eap/EAP-web.htm, 2004.

[8] E.J. McCormick, "Human Factors in Engineering and Design", McGraw-Hill, 1976.

[9] Online content available at: http://ndeaa.jpl.nasa.gov/nasa-nde/lommas/eap/actuators-comp.pdf, 2004.

[10] K. Youcef-Toumi, "Deisgn and Control of Direct-Drive Robots – a Survey", O. Khatib, J. Craig & Lozano Perez Eds, *The Robotics Review 1,* The MIT Press, 1989, pp.283-302.

[11] N. Hogan and E. Colgate, "Stability Problems in Contact Tasks", O. Khatib, J. Craig & Lozano Perez Eds, *The Robotics Review 1,* The MIT Press, 1989, pp.339-348.

[12] J.Paine, "Piezoelectric Step and Repeat Hydraulic Motor Phase I STTR", online content available at: http://www.darpa.mil/dso/thrust/matdev/chap/briefings/timchap2000day1/Paine_PiezoStep.pdf, 1999.

[13] Online content available at: http://www.consult-g2.com/papers/paper15/paper.html.

[14] Honda Motor Company, Online content available at: http://world.honda.com/ASIMO/P3/spec/, 2004.

[15] Gill Pratt, "Biologically Inspired Components of Robots – Sensors, Actuators and Power Supplies", unpublished, 2002.

[16] J.J. E. Slotine, W. Li, "Applied Nonlinear Control", Prentice-Hall, 1986.